

Halftone Image Watermarking by Content Aware Double-Sided Embedding Error Diffusion

Yuanfang Guo[✉], Member, IEEE, Oscar C. Au, Fellow, IEEE, Rui Wang, Member, IEEE,
Lu Fang, Senior Member, IEEE, and Xiaochun Cao, Senior Member, IEEE

Abstract—In this paper, we carry out a performance analysis from a probabilistic perspective to introduce the error diffusion-based halftone visual watermarking (EDHVW) methods' expected performances and limitations. Then, we propose a new general EDHVW method, content aware double-sided embedding error diffusion (CaDEED), via considering the expected watermark decoding performance with specific content of the cover images and watermark, different noise tolerance abilities of various cover image content, and the different importance levels of every pixel (when being perceived) in the secret pattern (watermark). To demonstrate the effectiveness of CaDEED, we propose CaDEED with expectation constraint (CaDEED-EC) and CaDEED-noise visibility function (NVF) and importance factor (IF) (CaDEED-N&I). Specifically, we build CaDEED-EC by only considering the expected performances of specific cover images and watermark. By adopting the NVF and proposing the IF to assign weights to every embedding location and watermark pixel, respectively, we build the specific method CaDEED-N&I. In the experiments, we select the optimal parameters for NVF and IF via extensive experiments. In both the numerical and visual comparisons, the experimental results demonstrate the superiority of our proposed work.

Index Terms—Halftone image, watermarking, halftone visual watermarking, optimization, noise tolerance ability.

I. INTRODUCTION

PRINTED material, such as newspapers, books, magazines etc., has been widely employed in the distribution of multimedia content for multiple decades. Although distributing

Manuscript received November 11, 2016; revised November 16, 2017; accepted February 28, 2018. Date of publication March 12, 2018; date of current version April 12, 2018. This work was supported in part by the National Key Research and Development Program of China under Grant 2016YFC0801004, in part by the National Natural Science Foundation of China under Grant 61722209, Grant 61332012, Grant U1605252, and Grant 61331015, in part by the Fundamental Theory and Cutting Edge Technology Research Program of Institute of Information Engineering, CAS, under Grant Y7Z0381102, and in part by the Foundation of Science and Technology on Information Assurance Laboratory under Grant KJ-17-006. The associate editor coordinating the review of this manuscript and approving it for publication was Prof. Patrick le Callet. (*Corresponding author: Rui Wang.*)

Y. Guo is with the State Key Laboratory of Information Security, Institute of Information Engineering, Chinese Academy of Sciences, Beijing 100093, China, and also with the Science and Technology on Information Assurance Laboratory, Beijing 100072, China (e-mail: eandyguo@connect.ust.hk).

O. C. Au is with Origin Wireless Inc., Greenbelt, MD 20770 USA (e-mail: eaau90@gmail.com).

R. Wang and X. Cao are with the State Key Laboratory of Information Security, Institute of Information Engineering, Chinese Academy of Sciences, Beijing 100093, China, and also with the School of Cyber Security, University of Chinese Academy of Sciences, Beijing 100049, China (e-mail: wangrui@iie.ac.cn; caoxiaochun@iie.ac.cn).

L. Fang is with the Tsinghua-Berkeley Shenzhen Institute, Tsinghua University, Shenzhen 518057, China (e-mail: fanglu@sz.tsinghua.edu.cn).

Color versions of one or more of the figures in this paper are available online at <http://ieeexplore.ieee.org>.

Digital Object Identifier 10.1109/TIP.2018.2815181

multimedia content in digital versions has been very popular in recent years, printed material is still playing an important role. Due to the explosive usage of digital and printed multimedia content, multimedia security issues have arisen quickly in recent years. In general, to protect a multimedia content, not only should the digital versions of the multimedia content be protected, but also the printed versions. Since most of the techniques, which protects the digital versions, cannot be directly applied to the printed versions, halftone image watermarking has been specially developed for protecting the printed versions of multimedia content over the past two decades. Numerous issues still exist and the proposed work is developed for resolving some of the problems.

The paper is organized as follows. Section I-A introduces watermarking and halftoning. Section I-B presents a literature review. Section I-C briefs the reader about the motivations and contributions of the paper. Section II recalls three highly related methods. Section III presents the performance analysis to the error diffusion based halftone visual watermarking (EDHVW) methods from a probabilistic perspective. Section IV proposes the new method. Section V gives the experimental results. Finally, the conclusion is drawn in Section VI.

A. Introduction of Watermarking and Halftoning

First of all, watermarking and halftoning (and the halftone image) will be introduced respectively.

In watermarking, a message called a watermark is embedded into another message called the cover message to generate another message called a stego message, which is similar to the cover message. The watermark can typically be decoded by processing the stego message. The message may be an image, video, audio, speech or other media content. This paper is focused on image watermarking. In most applications, image watermarks are invisible in the stego images, though they can be visible sometimes. Some watermarks are designed to be fragile [1]–[4], such that they are easily broken when edited, as is typically required for authentication. Others are designed to be robust [5]–[9], such that they can not be easily removed when edited, as is typically required in copyright protection. Still more are designed for data hiding [10]–[12] with no specific fragileness or robustness requirements, as in steganography. Further watermarks are designed to be private where the original cover message is needed during watermark decoding, while some are public as the original cover message is not needed in watermark decoding.

Halftoning is a special image processing technique to print images on printed material. Usually, only two tones (for printing grayscale images) are available in printed material: white from the color of the paper and black from the ink. Grayscale halftoning uses just 1 bit (black and white) to approximate the original 8-bit grayscale image such that, when viewed from a certain distance, the grayscale halftone image will resemble the original grayscale image. Color halftoning [13] and multilevel halftoning [14] possess similar mechanism. Nowadays, there are several classes of halftoning methods: ordered dithering [15], error diffusion [16]–[18], dot diffusion [19]–[22] and direct binary search [23]–[26].

B. Previous Work

Most regular watermarking methods for grayscale images, such as Least Significant Bit embedding [27], cannot be effectively performed on halftone images, because of the 1-bit nature of halftone images mentioned above. Therefore, researchers pay various attentions to this special area, halftone image watermarking.

In general, halftone image watermarking methods can be classified into two classes. The Class 1 methods [28]–[33] embed a secret binary bitstream into a single halftone image (with both the cover and stego images being halftone images) and the embedded bitstream can be extracted later by applying a certain algorithm (with respective to the embedding algorithm) to the stego image. The Class 2 methods [34]–[38] embed a secret pattern (watermark) into multiple halftone images (with N stego halftone images obtained from N cover halftone images, $N > 1$, N usually equals 2), such that when the stego halftone images are overlaid or the not-exclusive-or operation is performed, the secret pattern will be revealed. As mentioned in [39], halftone visual watermarking (HVW) is employed to represent the Class 2 methods. Since HVW methods usually perform embedding during the halftoning process, most of the HVW methods are designed based on different halftoning methods and thus they can be further classified into different categories. Among the HVW methods, error diffusion based HVW (EDHVW) methods drew most of the researchers' attentions due to the fact that error diffusion, which generates halftone images with good visual quality while remains simple implementation procedures, are widely adopted during the past forty years.

Among the EDHVW methods, in 2001, Fu and Au [40] proposed the first method called DHSED (Data Hiding by Stochastic Error Diffusion) to embed a secret pattern in two halftone images generated using stochastic error diffusion. In 2003, Fu and Au [41] proposed another method called Data Hiding by Conjugate Error Diffusion (DHCED) which imposes conjugate properties in the two stego halftone images according to the watermark pattern and improves the previous poor performance [40] significantly. Pei and Guo [42] proposed to shift the quantization threshold, which provided a similar performance compared to [41]. In 2006, Chang *et al.* [43] proposed to firstly adjust the dynamic range of the original grayscale image and then employ pattern lookup and pixel swapping to perform embedding. The contrast of

the revealed secret pattern was low and the visual quality of the stego images was quite poor compared to the original images, though the details of the embedded halftone image was preserved with this method. In 2008, Yang et al. found that when applying the gradient attacks to the stego images generated by DHCED [41], some visual boundaries of the secret pattern appeared in the edge map. Thus, they proposed in [44] to extend traditional visual cryptography. However, the visual quality of the second generated stego image dropped obviously compared to their first generated image. Also, the contrast of the revealed secret pattern in [44] was much lower than that in [41], which makes it inconvenient for the users to distinguish the secret pattern from the background. In 2011, Guo and Tsai [46] improves the method in [42] by adaptively shifting the quantization threshold. Unfortunately, their performance is highly depending on the lookup table training results. Meanwhile, we analyzed the advantages and weaknesses of the approach in [41] and then proposed Data Hiding by Dual Conjugate Error Diffusion (DHDCE) in [45], which makes amendments to both stego halftone images rather than only the second halftone image. The experimental results in [45] show that DHDCE improved the performance significantly. Recently, we proposed to tackle the HVW problems from a theoretical approach in [39] by proposing a general formulation for HVW problems. Then the general formulation is applied to two specific EDHVW problems by proposing two general methods, named Single-sided Embedding Error Diffusion (SEED) and Double-sided Embedding Error Diffusion (DEED). If the L-2 Norm is selected in DEED, DEED(L-2) can achieve better performances compared to previous methods. Still, DEED possesses weaknesses. It actually assumes that the identical amount of embedding distortions for different pixel locations are equally perceived and every pixel in the secret pattern is equally important.

C. Motivations and Contributions

Although many EDHVW methods are developed in the past years as introduced in Section I-B, no general performance analysis has been performed except the specific analysis to DHSED and DHCED in [41]. Inspired by [41], we give a general analysis to the typical EDHVW methods in this paper. According to our analysis, the performance of EDHVW methods are limited by the cover image content. More embedding distortions, which are less demanded intuitively, are likely required when the EDHVW methods embed the secret patterns into the bright/dark image regions to achieve a high correct decoding rate.

Besides of the problem above, the assumption of DEED also exists in most of the previous methods, while in reality, identical distortions may be perceived quite differently due to the different cover image content. Also, the watermark pixels, which contains more structural information, tends to be more important than others when considering the effect of human perception in the HVW decoding procedure, i.e. the structural information tends to be more sensitive to the human eyes intuitively. If identical certain amount of watermark decoding distortions is considered, distortions to the structural

pixels (especially for the pixels in the fine texture regions) may significantly degrade the human perceived watermark information, while the distortions at the flat regions usually affect less when human perceives the decoded image. Under such circumstances, we propose a new general EDHVV method called Content aware Double-sided Embedding Error Diffusion (CaDEED). The detailed contributions are as follows:

- 1: We theoretically analyze the expected performances and limitations of the EDHVV methods from a probabilistic perspective. The analysis indicates that the performances of EDHVV methods are highly related to the content of the cover images.
- 2: According to the analysis, we propose to formulate the watermark decoding distortions, i.e. the differences between the extracted and reference watermarks, with a linear combination of two models. One is the traditional difference between the decoded and original watermark. The other is our proposed model, the difference between the decoded and expected watermark calculated from the cover images' content and the original watermark.
- 3: With the new model of the watermark decoding distortions, we propose a new general EDHVV method called CaDEED by further assigning different weights to the embedding distortions according to the different cover image content and the differences between the reference and revealed secret pattern. With the problem formulation of CaDEED, we solve the optimization problem to obtain a relaxed optimal solution.
- 4: To better demonstrate CaDEED, we propose two specific schemes, CaDEED with expectation constraint (CaDEED-EC) and CaDEED-NVF&IF (CaDEED-N&I). CaDEED-EC only considers the expected performances with specific content of the cover images and watermark. CaDEED-N&I adopts the classical noise visibility function (NVF) [47] to calculate the weights for the embedding distortions. We also propose a simple yet effective method to calculate the weights for the watermark decoding distortions, i.e. the importance factors (IF) for each pixel in the secret pattern.
- 5: In the experiments, the parameters in CaDEED-N&I are firstly selected via extensive experiments. Then we propose a new measurement which considers the watermark content and better quantifies the differences between the proposed method and previous methods. For better measuring the performances of the EDHVV methods, we also modify the traditional image distortion measure Peak Signal-to-Noise Ratio (PSNR) via considering the cover image content. By employing both the existing and new measurements, we demonstrate that our proposed work outperforms both classical and latest EDHVV methods obviously.

II. BACKGROUNDS

In this section, three previous important EDHVV methods, DHCED, DHDced and DEED, will be introduced respectively.

Here some common notations, which will be employed throughout this paper, is introduced. Let X_1 and X_2 be the

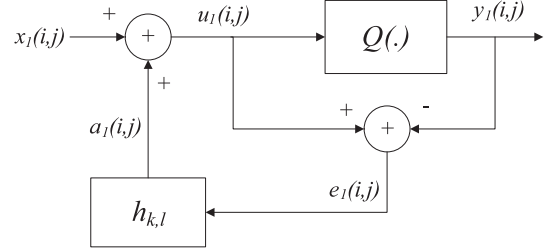


Fig. 1. Error Diffusion system.

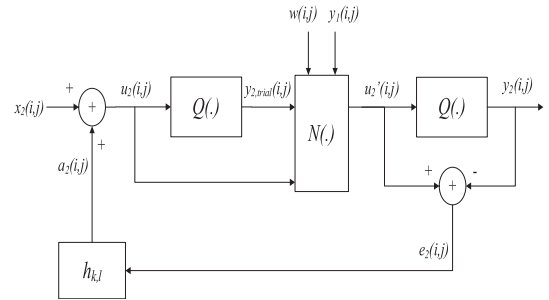


Fig. 2. DHCED system.

original grayscale images, which can be identical or different. Let Y_1 and Y_2 be the generated stego halftone images, W be the secret binary pattern to be embedded, W_w be the collection of locations of the white pixels in W , and W_b be the collection of locations of the black pixels in W . Let \otimes represent the binary AND operation, and let \odot be the binary not-exclusive-or (XNOR) operation.

The goal of DHCED, DHDced and DEED is to generate Y_1 and Y_2 from X_1 and X_2 , such that, when Y_1 and Y_2 are overlaid (performed XNOR operation between them) to reveal $Y_1 \otimes Y_2$, it will resemble W .

A. DHCED

In DHCED, Y_1 is generated by performing regular error diffusion on X_1 , as shown in Fig. 1 and the regular error diffusion process is described by Eqs. (1)-(3).

$$u_1(i, j) = x_1(i, j) + \sum h(k, l) \times e_1(i - k, j - l), \quad (1)$$

$$y_1(i, j) = \begin{cases} 0, & u_1(i, j) < 128 \\ 255, & u_1(i, j) \geq 128 \end{cases} \quad (2)$$

$$e_1(i, j) = u_1(i, j) - y_1(i, j), \quad (3)$$

where $u_1(i, j)$ is the sum of the current pixel value $x_1(i, j)$ and the past error (diffused from past pixels) to be carried by the current pixel, $h(k, l)$ is the error diffusion kernel and $e_1(i, j)$ is the error generated when processing the current pixel. Note that the to-be-diffused error $e_1(i, j)$, i.e. the quantization error, is defined as the difference between $u_1(i, j)$ and $y_1(i, j)$. Two common error diffusion kernels are the Steinberg kernel [16] and Jarvis kernel [17].

After obtaining Y_1 , the second halftone image Y_2 is generated by applying the DHCED system referencing to X_2 , Y_1 and W , and the DHCED system is shown in Fig. 2. For $(i, j) \in W_b$, $y_2(i, j)$ will be ‘favored’ to be conjugate to $y_1(i, j)$, and the ‘favor’ mechanism will be explained later. For $(i, j) \in W_w$, if $X_1 = X_2$, then $y_2(i, j) = y_1(i, j)$ will

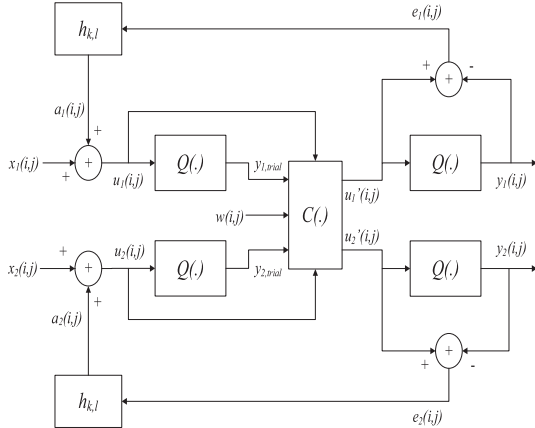


Fig. 3. DHDCEDE system.

be forced to be carried out. If $X_1 \neq X_2$, then $y_2(i, j)$ will be favored to be identical to $y_1(i, j)$.

The ‘favor’ mechanism works as follows. The DHCED system will perform a trial quantization on $u_2(i, j)$. Then if $y_2(i, j) \neq y_1(i, j) \oplus w(i, j)$, where $y_1(i, j) \oplus w(i, j)$ is the favored value of $y_2(i, j)$, the minimum distortion $\Delta u(i, j)$ to toggle the current pixel is calculated. If the minimum distortion is acceptable, i.e. $\Delta u(i, j) \leq T$, then the toggling will be performed. The threshold T controls the tradeoff between the contrast of the revealed secret pattern and the visual quality of the stego halftone image Y_2 . As T increases, the contrast of the revealed secret pattern increases and the visual quality of the stego halftone image Y_2 decreases.

B. DHDCEDE

Although DHCED gives good performance, it still possesses weaknesses. A certain type of artifacts called boundary artifact will appear in Y_2 , and are mainly located in the flat regions at the bottom and right boundaries of the locations where (i, j) is co-located in W_b when $X_1 = X_2$. If the Sobel filter is applied to Y_2 , the boundary artifacts will be more obvious on the edge map obtained.

To reduce the boundary artifacts and improve the performance of the watermarking technique, we proposed DHDCEDE which performs amendments when generating both Y_1 and Y_2 . The DHDCEDE system is shown in Fig. 3.

In DHDCEDE, Y_1 and Y_2 are generated simultaneously. For $(i, j) \in W_b / W_w$, DHDCEDE will firstly perform trial quantization on $u_1(i, j)$ and $u_2(i, j)$. Then two minimum distortions will be computed according to the strategies below.

Strategy 1:

Obtain $\Delta u_2(i, j)$ when $y_2(i, j)$ is favored to be conjugate/identical to $y_1(i, j)$.

Strategy 2:

Obtain $\Delta u_1(i, j)$ when $y_1(i, j)$ is favored to be conjugate/identical to $y_2(i, j)$.

After $\Delta u_1(i, j)$ and $\Delta u_2(i, j)$ have been calculated, the strategy causing the smaller distortion is selected. Similar to DHCED, T is also exploited during the calculations of $\Delta u_1(i, j)$ and $\Delta u_2(i, j)$ to control the distortion to be acceptable by the user. Note that when $X_1 = X_2$, DHDCEDE will force $y_1(i, j)$ and $y_2(i, j)$ to be identical.

C. DEED

In [39], we proposed a general formulation for general HVW problems as Eq. (4) shows.

$$\min D_h + \lambda * D_w, \quad (4)$$

where D_h stands for the distortion caused during the watermark embedding process, and D_w stands for the difference between the decoded watermark and the original watermark, $\lambda \leq 0$.

After Eq. (4) was proposed, two specific EDHVW problems were solved by applying this general formulation. The two problems will both generate and embed a secret pattern (watermark) W into two halftone images, Y_1 and Y_2 , such that when the stego images are overlaid or an XNOR operation is carried out between them, the secret pattern is revealed. In these two problems, one only embeds the secret pattern into one out of two cover images (solved by the general method SEED), while the other embeds the secret pattern into both cover images (solved by the general method DEED). According to the results in [39], DEED gives obviously better results compared to SEED, thus only DEED will be briefly introduced here due to limited space.

In DEED, to perform the necessary toggling to change the output halftone value, a distortion $\Delta u_{1,i}$ is added to $x_{1,i}$ and a distortion $\Delta u_{2,i}$ is added to $x_{2,i}$ to change the pixel values before quantization. By letting ΔU_1 and ΔU_2 be the distortions to be added to X_1 and X_2 during the watermark embedding process and $ED(\cdot)$ be the regular error diffusion process, DEED can be formulated as Eq. (5) shows.

$$\begin{aligned} \min_{\Delta U_1, \Delta U_2} & ||\Delta U_1||_p^p + ||\Delta U_2||_p^p + \lambda \cdot ||W \\ & - (ED(\mathbf{X}_1 + \Delta U_1) \circ ED(\mathbf{X}_2 + \Delta U_2))||_p^p, \end{aligned} \quad (5)$$

where ‘o’ stands for the decoding operation which can be either the AND operation (\otimes) or XNOR operation (\odot).

To our best knowledge, Eq. (5) can not be solved directly. Even brute force will have problems since as the image size goes up the possible solution set increases exponentially. However, this optimization problem can be relaxed and then solved accordingly. If we assume the regular error diffusion processing order is from the first pixel $x_{1,1}(x_{2,1})$ to the last pixel $x_{1,N}(x_{2,N})$, where N is the number of pixels in $X_1(X_2)$, and Y_1 and Y_2 are generated simultaneously, Eq. (5) can be reformed and relaxed to Eqs. (6) and (7).

$$\begin{aligned} J_1 = \min_{\Delta u_{1,1}, \Delta u_{2,1}} & \{|\Delta u_{1,1}|^p + |\Delta u_{2,1}|^p \\ & + \lambda \cdot |ed(x_{2,1} + \Delta u_{2,1}) \circ ed(x_{1,1} + \Delta u_{1,1}) - w_1|^p\}, \end{aligned} \quad (6)$$

$$\begin{aligned} J_n = \min_{\Delta u_{1,n}, \Delta u_{2,n}} & \{|\Delta u_{1,n}|^p + |\Delta u_{2,n}|^p \\ & + \lambda \cdot |ed(x_{2,n} + \Delta u_{2,n}) \circ ed(x_{1,n} + \Delta u_{1,n}) - w_n|^p \\ & + J_{n-1}\}, \end{aligned} \quad (7)$$

where $n \in \{2, 3, \dots, N\}$, and J_1 and J_n are the minimum cost obtained by the optimization process. Then the relaxed optimization problem can be solved easily by calculating the best $\Delta u_{1,i}$ and $\Delta u_{2,i}$ for the current pixels $x_{1,i}$ and $x_{2,i}$ and

the final stego halftone images Y_1 and Y_2 can be generated by simply performing regular error diffusion on $X_1 + \Delta U_1$ and $X_2 + \Delta U_2$ respectively. According to the results in [39], when the L-2 Norm is employed in DEED, its performance is superior compared to previous methods. Thus, DEED(L-2), as the latest EDHVW approach, will be compared in the experiments in the latter section.

III. PERFORMANCE ANALYSIS OF EDHVW METHODS

Based on our past experience, error diffusion based HVW (EDHVW) methods usually perform differently on different cover images. The performance is limited when certain cover images are employed, which is caused by the limited degree of freedom of halftone images. If users still demand a relatively high correct decoding rate, the embedding distortion will be excessive. In this section, we will introduce the expected performances and limitations of EDHVW methods from a probability perspective by generalizing the analysis of DHSED and DHCED in [41].

During the analysis, X_1 and X_2 will always be the original grayscale images. Y_1 and Y_2 are the two stego halftone images. In this section, the subscriptions O and N stand for AND operation and XNOR operation respectively.

Although EDHVW methods will embed a secret pattern into two or more halftone images, here the situation of two stego halftone images will be considered and introduced, as the analysis can be easily implied to the situations of more than two stego halftone images.

Before analyzing EDHVW methods, we will discuss the regular error diffusion first. In error diffusion, the halftoning technique tends to preserve the local intensity of the original grayscale image. Consider a rectangular region R_1 around (i, j) in X_1 has a constant intensity A and the co-located region R_2 around (i, j) in X_2 has a constant intensity B , where X_1 may or may not be identical to X_2 . Assume the left half of the region is in the white region W_w of W . Similarly, assume the right half of the region is in the black region W_b of W . If regular error diffusion is applied to X_1 to generate $Y_{1,ED}$, the probability distribution of the halftone pixel $y_{1,ED}(i, j)$ is

$$P[y_{1,ED}(i, j) = 255] = \frac{A}{255}, \quad (8)$$

$$P[y_{1,ED}(i, j) = 0] = \frac{255 - A}{255}. \quad (9)$$

The expectation of $y_{1,ED}(i, j)$ for $(i, j) \in R_1$ is

$$\begin{aligned} E[y_{1,ED}(i, j)] &= 0 \cdot P[y_{1,ED}(i, j) = 0] \\ &\quad + 255 \cdot P[y_{1,ED}(i, j) = 255] \\ &= 0 \cdot \frac{255 - A}{255} + 255 \cdot \frac{A}{255} \\ &= A, \end{aligned} \quad (10)$$

Therefore, the percentages of black and white pixels in $Y_{1,ED}$ in R_1 are $A/255 \cdot 100\%$ and $(255 - A)/255 \cdot 100\%$ respectively and the pixels are distributed evenly in R_1 .

Assume that when a EDHVW method embeds the secret pattern, the distortion during the embedding process is reasonably small, then the average intensity in R_1 and R_2 could still

be approximately A and B respectively. Then the probability distributions of the stego halftone pixels $y_1(i, j)$ and $y_2(i, j)$ are

$$P[y_1(i, j) = 255] \approx \frac{A}{255}, \quad (11)$$

$$P[y_1(i, j) = 0] \approx \frac{255 - A}{255}, \quad (12)$$

$$P[y_2(i, j) = 255] \approx \frac{B}{255}, \quad (13)$$

$$P[y_2(i, j) = 0] \approx \frac{255 - B}{255}. \quad (14)$$

The expectations of $y_1(i, j)$ for $(i, j) \in R_1$, $y_2(i, j)$ for $(i, j) \in R_2$ are

$$\begin{aligned} E[y_1(i, j)] &= 0 \cdot P[y_1(i, j) = 0] + 255 \cdot P[y_1(i, j) = 255] \\ &\approx 0 \cdot \frac{255 - A}{255} + 255 \cdot \frac{A}{255} \\ &= A, \end{aligned} \quad (15)$$

$$\begin{aligned} E[y_2(i, j)] &= 0 \cdot P[y_2(i, j) = 0] + 255 \cdot P[y_2(i, j) = 255] \\ &\approx 0 \cdot \frac{255 - B}{255} + 255 \cdot \frac{B}{255} \\ &= B. \end{aligned} \quad (16)$$

The percentages of black and white pixels in R_1 in Y_1 are approximately $A/255 \cdot 100\%$ and $(255 - A)/255 \cdot 100\%$. The percentages of black and white pixels in R_2 in Y_2 are approximately $B/255 \cdot 100\%$ and $(255 - B)/255 \cdot 100\%$.

Let Y_A be the overlay/AND operation decoded image. Then $y_A(i, j)$ is 255 if and only if $y_1(i, j) = y_2(i, j) = 255$. Let Y_O be the XNOR operation decoded image. If $y_1(i, j) = y_2(i, j)$, $y_O(i, j)$ will be 0. Otherwise $y_O(i, j) = 255$.

In the left half of R_1 and R_2 , which are in W_w , $y_1(i, j)$ and $y_2(i, j)$ are favored to be identical to each other such that $y_1(i, j)$ and $y_2(i, j)$ tend to be black and white at the same time. Similarly, in the right half of R_1 and R_2 , which are in W_b , $y_1(i, j)$ and $y_2(i, j)$ are favored to be conjugate to each other such that $y_1(i, j)$ and $y_2(i, j)$ tend not to be black at the same time.

The analysis for the detailed cases in $(i, j) \in W_w$ and $(i, j) \in W_b$ are omitted here for convenience. Please refer to the appendix for detailed derivations.

The analysis can be summarized in Eqs. (17)-(22), which present the expected values and contrast for the AND operation and XNOR operation decoded images in an ideal situation. For $(i, j) \in W_w$, the expected values of $y_A(i, j)$ and $y_O(i, j)$ are

$$E[y_A(i, j)|(i, j) \in W_w] \approx 255 - \min(A, B), \quad (17)$$

$$E[y_O(i, j)|(i, j) \in W_w] \approx 255 - |A - B|. \quad (18)$$

For $(i, j) \in W_b$, the expected values of $y_A(i, j)$ and $y_O(i, j)$ are

$$E[y_A(i, j)|(i, j) \in W_b] \approx \begin{cases} 0, & A + B \leq 255 \\ A + B - 255, & A + B > 255 \end{cases} \quad (19)$$

$$E[y_O(i, j)|(i, j) \in W_b] \approx |(A + B) - 255|. \quad (20)$$

The contrasts between the left halves and the right halves of R , which are generated by AND operation and XNOR operation, are

$$Cs_A \approx \begin{cases} 1, & A + B \leq 255 \\ 1 - \frac{A + B - 255}{255 - \min(A, B)}, & A + B > 255 \end{cases} \quad (21)$$

$$Cs_O \approx \frac{255 - |A - B| - |(A + B) - 255|}{255 - |A - B|}. \quad (22)$$

The above equations give the expected performances and limitations of EDHVV methods, where the expected performances are highly depending on the content of the cover images and watermark. In practice, the specific decoding results may exceed the theoretical limits if certain embedding distortions are allowed.

IV. CONTENT AWARE DOUBLE-SIDED EMBEDDING ERROR DIFFUSION

According to the analysis in Section III, the performances of the EDHVV methods are affected by the specific content of the cover images and the secret pattern. To achieve a relatively high correct decoding rate, more embedding distortions, which are less desired, are demanded for the dark/bright cover image regions compared to others. Unfortunately, to our best knowledge, the existing methods, such as DEED in [39], DHDCED in [45] and DHCED in [41], never consider this issue. Besides, the majority of the EDHVV methods including the latest method DEED have not considered the effect of human perception when formulating the embedding distortions and the differences between the reference and decoded secret pattern, though it formulate and solve the specific EDHVV problem decently. Therefore, we improve the problem formulation of DEED and propose a new general method, Content aware Double-sided Embedding Error Diffusion (CaDEED) by considering the content of the cover images and the secret pattern. Note that the definition of D_w in Eq. (4) is amended here from the differences between the original and decoded watermark to the differences between the reference and decoded watermark, for more generalization.

The existing EDHVV methods only measure the difference between the original and decoded secret pattern. They never consider the performance limitations caused by the content of the cover images and the secret pattern. To achieve a high watermark correct decoding rate, they tend to induce more embedding distortions to the dark/bright image regions, which may further increase the risk of artifact appearances (the traces of the embedded secret pattern) and result in more image quality degradations to the stego images. To better formulate the differences between the reference and decoded secret pattern, by considering the expected performances of specific content of the cover images and the secret pattern, we propose to define D_w in a more general approach as Eq. (23) shows.

$$D_w = ||\alpha * |\mathbf{W} - (\mathbf{Y}_1 \circ \mathbf{Y}_2)|^p + \beta * |\mathbf{EP} - (\mathbf{Y}_1 \circ \mathbf{Y}_2)|^p||_1, \quad (23)$$

where $EP = E[(\mathbf{Y}_1 \circ \mathbf{Y}_2)]$ stands for the expected decoded secret pattern calculated via Eqs. (17)-(20), \mathbf{EP} , \mathbf{Y}_1 , \mathbf{Y}_2 and

\mathbf{W} stand for the vector form of EP , \mathbf{Y}_1 , \mathbf{Y}_2 , \mathbf{W} and each of them contains N elements, and α and β are the assigned weights for controlling the tradeoff between the two calculated similarities. When β/α increases, the proposed model favors the decoded secret pattern to be more similar to the expected decoded secret pattern and vice versa.

Different content of the cover images and the secret pattern not only gives different performances, but also affects the human perceived results. Previously, DHCED, DHDCED and DEED all treat the distortions caused during the embedding process as equally important for every pixel in the stego images. In fact, according to the human visual system (HVS), different image gives different perceived content if identical distortions are added. In this paper, since we are embedding the secret pattern by amending both \mathbf{Y}_1 and \mathbf{Y}_2 , we define the weighted distortions caused during the embedding process D_h as Eq. (24) shows.

$$\begin{aligned} D_h = D_{Y_1} + D_{Y_2} &= ||\mathbf{M}_1 * |\mathbf{X}_1 - (\mathbf{X}_1 + \Delta \mathbf{U}_1)|^p||_1 \\ &\quad + ||\mathbf{M}_2 * |\mathbf{X}_2 - (\mathbf{X}_2 + \Delta \mathbf{U}_2)|^p||_1 \\ &= ||\mathbf{M}_1 * |\Delta \mathbf{U}_1|^p||_1 + ||\mathbf{M}_2 * |\Delta \mathbf{U}_2|^p||_1, \end{aligned} \quad (24)$$

where \mathbf{M}_1 , \mathbf{M}_2 , \mathbf{X}_1 , \mathbf{X}_2 , $\Delta \mathbf{U}_1$ and $\Delta \mathbf{U}_2$ stand for the vector form of M_1 , M_2 , X_1 , X_2 , ΔU_1 and ΔU_2 and each of them contains N elements. Note that M_1 and M_2 are masks which assign weights to different distortions at different locations, i.e. different distortion tolerance ability according to different image content. M_1 and M_2 can be calculated via any specific method.

For the secret pattern, researchers used to treat every pixel equally. From our observation, different pixels in the secret pattern tend to have different levels of importance. The pixels, which contain more structural information, tend to be more important than other pixels, because human eyes are more sensitive to the structural information. Besides, if those pixels can not be correctly decoded, users can only perceive partial or even undistinguishable decoded secret pattern. In the worst case, the secret pattern can hardly be recognized correctly. Therefore, in CaDEED, the weighted differences between the reference and decoded secret pattern are defined as Eq. (25) shows.

$$\begin{aligned} D_w = ||\Psi * (\alpha * |\mathbf{W} - (\mathbf{Y}_1 \circ \mathbf{Y}_2)|^p &+ \beta * |\mathbf{EP} - (\mathbf{Y}_1 \circ \mathbf{Y}_2)|^p)||_1, \end{aligned} \quad (25)$$

where Ψ stand for the vector form of Ψ and contains N elements. Note that Ψ assigns weight to different pixels in the secret pattern and it can also be calculated via any specific method.

The two stego halftone images \mathbf{Y}_1 and \mathbf{Y}_2 can be generated by Eqs. (26) and (27) by letting $ED(\cdot)$ be the regular error diffusion which is described in Fig. 1.

$$\mathbf{Y}_1 = ED(\mathbf{X}_1 + \Delta \mathbf{U}_1) \quad (26)$$

$$\mathbf{Y}_2 = ED(\mathbf{X}_2 + \Delta \mathbf{U}_2) \quad (27)$$

By substituting Eq. (24), (25), (26) and (27) into Eq. (4),

CaDEED can be described as Eq. (28) shows.

$$\begin{aligned} \min_{\Delta \mathbf{U}_1, \Delta \mathbf{U}_2} & ||\mathbf{M}_1 * |\Delta \mathbf{U}_1|^p||_1 + ||\mathbf{M}_2 * |\Delta \mathbf{U}_2|^p||_1 \\ & + \lambda * ||\Psi * (\alpha * |\mathbf{W} - (\mathbf{Y}_1 \circ \mathbf{Y}_2)|^p \\ & + \beta * |\mathbf{EP} - (\mathbf{Y}_1 \circ \mathbf{Y}_2)|^p)||_1 \end{aligned} \quad (28)$$

The solution to Eq. (28) is essentially the global optimum solution of CaDEED's problem. However, to our best knowledge, there is no closed-form solution to Eq. (28) due to the unique property of halftone images and the error diffusion process. Since the size of the possible solutions set increases exponentially as the image size increases, brute force also cannot be applied. Fortunately, by applying a similar optimization method as in [39], we can manage to find a relaxed optimal solution to Eq. (28) as follows.

In error diffusion process, there exists a feedback loop. Then, latter generated halftone pixels are depending on former pixels. Thus the distortions to be added to the latter pixels are also depending on previous distortions as shown in Eq. (29) which is obtained by rewriting Eq. (28) using the elements instead of vectors and considering the dependencies among the elements.

$$\begin{aligned} \min_{\Delta u_{1,1}, \Delta u_{1,2}, \dots, \Delta u_{1,N}, \Delta u_{2,1}, \Delta u_{2,2}, \dots, \Delta u_{2,N}} & \left\{ \sum_{i=1}^N \{|m_{1,i} * |\Delta u_{1,i}|^p| \right. \\ & + |m_{2,i} * |\Delta u_{2,i}|^p| \} + \lambda * \left\{ \sum_{i=1}^N |\psi_i * (\alpha * |ed(x_{2,i} + \Delta u_{2,i}) \right. \\ & \circ ed(x_{1,i} + \Delta u_{1,i}) - w_i|^p + \beta * |ed(x_{2,i} + \Delta u_{2,i}) \\ & \circ ed(x_{1,i} + \Delta u_{1,i}) - ep_i|^p| \} \} \end{aligned} \quad (29)$$

where $\forall i \in \{2, 3, \dots, N\}$, $\Delta u_{1,i}$ depends on $\{\Delta u_{1,1}, \dots, \Delta u_{1,i-1}\}$, $\forall i \in \{2, 3, \dots, N\}$, $\Delta u_{2,i}$ depends on $\{\Delta u_{2,1}, \dots, \Delta u_{2,i-1}\}$ and $ed(\cdot)$ stands for carrying out regular error diffusion, as described in Eqs. (1)-(3), on the current pixel and diffusing its quantization error to the latter pixels.

If we assume the regular error diffusion processing order is from 1 to N , the joint optimization problem in Eq. (29) can be reformed into ordered separate problems in Eq. (30).

$$\begin{aligned} \min_{\Delta u_{1,1}, \Delta u_{2,1}} & \left\{ \min_{\Delta u_{1,2}, \Delta u_{2,2}} \left\{ \dots \min_{\Delta u_{1,N}, \Delta u_{2,N}} \left\{ \sum_{i=1}^N \{|m_{1,i} * |\Delta u_{1,i}|^p| \right. \right. \right. \\ & + |m_{2,i} * |\Delta u_{2,i}|^p| \} + \lambda * \left\{ \sum_{i=1}^N |\psi_i * (\alpha * |ed(x_{2,i} + \Delta u_{2,i}) \right. \\ & \circ ed(x_{1,i} + \Delta u_{1,i}) - w_i|^p + \beta * |ed(x_{2,i} + \Delta u_{2,i}) \\ & \circ ed(x_{1,i} + \Delta u_{1,i}) - ep_i|^p| \} \} \dots \} \end{aligned} \quad (30)$$

For convenience, S_i in Eq. (31) is employed to represent the cost calculated when processing the i -th pixels of X_1 and X_2 .

$$\begin{aligned} S_i = & |m_{1,i} * |\Delta u_{1,i}|^p| + |m_{2,i} * |\Delta u_{2,i}|^p| \\ & + \lambda * |\psi_i * (\alpha * |ed(x_{2,i} + \Delta u_{2,i}) \circ ed(x_{1,i} + \Delta u_{1,i}) \\ & - w_i|^p + \beta * |ed(x_{2,i} + \Delta u_{2,i}) \circ ed(x_{1,i} + \Delta u_{1,i}) \\ & - ep_i|^p)|, \forall i \in \{1, 2, 3, \dots, N\}, \end{aligned} \quad (31)$$

where $\forall i \in \{2, 3, \dots, N\}$, S_i depends on $\{S_1, \dots, S_{i-1}\}$ since $\forall i \in \{2, 3, \dots, N\}$, Δu_i depends on $\{\Delta u_1, \dots, \Delta u_{i-1}\}$.

Then Eq. (30) can be reformed to Eq. (32) with Eq. (31).

$$\begin{aligned} \min_{\Delta u_{1,1}, \Delta u_{2,1}} & \{S_1 + \min_{\Delta u_{1,2}, \Delta u_{2,2}} \{S_2 + \dots \\ & + \min_{\Delta u_{1,N-2}, \Delta u_{2,N-2}} \{S_{N-2} + \min_{\Delta u_{1,N-1}, \Delta u_{2,N-1}} \{S_{N-1} \\ & + \min_{\Delta u_{1,N}, \Delta u_{2,N}} \{S_N\}\} \dots \} \} \} \end{aligned} \quad (32)$$

Currently, these separate problems' optimization order in Eq. (32) is from N to 1, which is inconsistent with the error diffusion processing order. To our best knowledge, due to the existing dependencies among all the variables, Eq. (32) can only be solved if the optimization order is relaxed to be consistent with the error diffusion processing order.

Since $\Delta u_{1,N}$ and $\Delta u_{2,N}$ depend on all previous variable distortions, Eq. (32) can be relaxed to Eq. (33) by relaxing the optimization order between the variable pairs $(\Delta u_{1,N}, \Delta u_{2,N})$ and $(\Delta u_{1,N}, \Delta u_{2,N})$.

$$\begin{aligned} \min_{\Delta u_{1,1}, \Delta u_{2,1}} & \{S_1 + \min_{\Delta u_{1,2}, \Delta u_{2,2}} \{S_2 + \dots \\ & + \min_{\Delta u_{1,N-2}, \Delta u_{2,N-2}} \{S_{N-2} + \min_{\Delta u_{1,N-1}, \Delta u_{2,N-1}} \{S_{N-1}\} \\ & + \min_{\Delta u_{1,N}, \Delta u_{2,N}} \{S_N\}\} \dots \} \} \end{aligned} \quad (33)$$

Then similar relaxations can be performed on the remaining joint optimization problem. If we continue to carry out relaxations, Eq. (34) can be finally obtained.

$$\begin{aligned} \min_{\Delta u_{1,1}, \Delta u_{2,1}} & \{S_1\} + \min_{\Delta u_{1,2}, \Delta u_{2,2}} \{S_2\} + \dots \\ & + \min_{\Delta u_{1,N-2}, \Delta u_{2,N-2}} \{S_{N-2}\} + \min_{\Delta u_{1,N-1}, \Delta u_{2,N-1}} \{S_{N-1}\} \\ & + \min_{\Delta u_{1,N}, \Delta u_{2,N}} \{S_N\} \end{aligned} \quad (34)$$

Then Eq. (34) can be reformed to Eq. (35) based on the processing order of regular error diffusion (from 1 to N).

$$\min_{\Delta u_{1,N}, \Delta u_{2,N}} \{ \dots \min_{\Delta u_{1,2}, \Delta u_{2,2}} \{ \min_{\Delta u_{1,1}, \Delta u_{2,1}} \{S_1\} + S_2 \} + \dots + S_N \} \quad (35)$$

Then Eq. (36) and (37) can be derived from Eqs. (35) and (31), and the variables can be easily solved from $(x_{1,1}, x_{2,1})$ to $(x_{1,N}, x_{2,N})$ once a pair.

$$\begin{aligned} C_1 = & \min_{\Delta u_{1,1}, \Delta u_{2,1}} \{ |m_{1,1} * |\Delta u_{1,1}|^p| + |m_{2,1} * |\Delta u_{2,1}|^p| \\ & + \lambda * |\psi_1 * (\alpha * |ed(x_{2,1} + \Delta u_{2,1}) \circ ed(x_{1,1} + \Delta u_{1,1}) \\ & - w_1|^p + \beta * |ed(x_{2,1} + \Delta u_{2,1}) \circ ed(x_{1,1} + \Delta u_{1,1}) \\ & - ep_1|^p)| \}, \end{aligned} \quad (36)$$

$$\begin{aligned} C_n = & \min_{\Delta u_{1,n}, \Delta u_{2,n}} \{ |m_{1,n} * |\Delta u_{1,n}|^p| + |m_{2,n} * |\Delta u_{2,n}|^p| \\ & + \lambda * |\psi_n * (\alpha * |ed(x_{2,n} + \Delta u_{2,n}) \circ ed(x_{1,n} + \Delta u_{1,n}) \\ & - w_n|^p + \beta * |ed(x_{2,n} + \Delta u_{2,n}) \circ ed(x_{1,n} + \Delta u_{1,n}) \\ & - ep_n|^p)| + C_{n-1} \}, \end{aligned} \quad (37)$$

where $n \in \{2, 3, \dots, N\}$ and C_1 and C_n are the minimum cost obtained during the optimization process.

With ΔU_1 and ΔU_2 solved according to Eq. (36) and (37), Y_1 and Y_2 can be obtained by Eq. (26) and (27), respectively.

In practice, CaDEED will calculate the optimal $\Delta u_{1,i}$ and $\Delta u_{2,i}$ for the current pixels $x_{1,i}$ and $x_{2,i}$ first. Then CaDEED will perform regular error diffusion on $x_{1,i} + \Delta u_{1,i}$ and $x_{2,i} + \Delta u_{2,i}$ separately. When calculating the optimal $\Delta u_{1,i}$ and $\Delta u_{2,i}$, the possible solutions set can be reduced to a much smaller set with only four possible solutions: (a) $\Delta u_{1,i} = \Delta u_{2,i} = 0$; (b) $\Delta u_{1,i} = 0$, $\Delta u_{2,i} \neq 0$; (c) $\Delta u_{2,i} = 0$, $\Delta u_{1,i} \neq 0$; (d) $\Delta u_{1,i} \neq 0$ and $\Delta u_{2,i} \neq 0$. Since the cost in option (d) is indeed larger or equal to the other three options, the final possible solution set contains three possible solutions. The CaDEED algorithm is shown in Algorithm 1.

Algorithm 1 CaDEED

Input: $\mathbf{X}_1, \mathbf{X}_2, \mathbf{W}, p, \lambda, \alpha, \beta, \circ$, the error diffusion kernel, the specific methods to calculate M_1, M_2, Ψ

Output: $\mathbf{Y}_1, \mathbf{Y}_2$

- 1: Obtain EP, M_1, M_2, Ψ .
- 2: **for** $i = 1$ to N **do**
- 3: Obtain $[\Delta u_{1,i} \Delta u_{2,i}] = \underset{\Delta u_{1,i}, \Delta u_{2,i}}{\operatorname{argmin}} S_i$ ▷ refer to (31)
- 4: $y_{1,i} = ed(x_{1,i} + \Delta u_{1,i})$
- 5: $y_{2,i} = ed(x_{2,i} + \Delta u_{2,i})$
- 6: **end for**
- 7: **return** $\mathbf{Y}_1, \mathbf{Y}_2$

In CaDEED, different parameters, M_1, M_2 and Ψ give different specific EDHVW method. Note that if $\alpha = 1, \beta = 0, M_1 = M_2 = 1$ and $\Psi = 1$, CaDEED is essentially equivalent to DEED. Besides, if a $\Delta U_1 = 0$ constraint is added to the formulation, CaDEED becomes a single-sided embedding algorithm. For example, if $\alpha = 1, \beta = 0, M_1 = M_2 = 1, \Psi = 1$ and a $\Delta U_1 = 0$ constraint is added to CaDEED, CaDEED is equivalent to SEED.

To demonstrate the effectiveness of CaDEED, CaDEED generates CaDEED with expectation constraint (CaDEED-EC), by selecting $\alpha = \beta = 1, M_1 = M_2 = 1$ and $\Psi = 1$. Besides of CaDEED-EC, CaDEED-NVF&IF (CaDEED-N&I) is also proposed with $\alpha = \beta = 1$. In this scheme, the Noise Visibility Function (NVF) [47] is selected to calculate M_1 and M_2 , and a simple yet effective method, which calculates different importance factors (IF) for different pixels, is proposed. According to DEED(L-2)'s experience [39], p is set to be 2.

The Noise Visibility Function [47] in CaDEED-N&I is described in Eqs. (38) and (39).

$$m_1(i, j) = v_1(i, j) = \frac{1}{1 + \theta_1 \sigma_{Rx_1}^2(i, j)}, \quad (38)$$

$$m_2(i, j) = v_2(i, j) = \frac{1}{1 + \theta_2 \sigma_{Rx_2}^2(i, j)}, \quad (39)$$

where Rx_1 and Rx_2 are the local neighborhoods centered at $x_{1,i}(i, j)$ and $x_{2,i}(i, j)$ respectively. $\sigma_{Rx_1}^2(i, j)$ and $\sigma_{Rx_2}^2(i, j)$ are the local variances for Rx_1 and Rx_2 respectively. θ_1, θ_2 are calculated as Eq. (40) and (41) show.

$$\theta_1 = \frac{D}{\sigma_{Rx_{1,max}}^2}, \quad (40)$$



Fig. 4. Lena's NVF masking image. To highlight the pixels which can tolerate more noise, here darker pixels represent the original pixels that possess weak noise tolerance ability, while brighter pixels represent the original pixels that possess high noise tolerance ability.

$$\theta_2 = \frac{D}{\sigma_{Rx_{2,max}}^2}, \quad (41)$$

where $\sigma_{Rx_{1,max}}^2$ and $\sigma_{Rx_{2,max}}^2$ are the maximum local variances in X_1 and X_2 respectively. $D = 75$ is an experimentally determined parameter.

NVF generates a masking image where the smaller a masking value is, the more noise the original pixel can tolerate compared to other pixels. An example is shown in Fig. 4. As we can observe, the texture regions can tolerate more noise compared to the smooth regions.

To calculate Ψ in CaDEED-N&I, we propose a simple but effective method to calculate a Importance Factor (IF) γ for each pixel in the secret pattern as Ψ . The calculation of γ is shown in Eq. (42).

$$\psi(i, j) = \gamma(i, j) = 1 + \frac{\sigma_{Rw}^2}{\sigma_{Rw_{max}}^2}, \quad (42)$$

where Rw is the local neighborhood centered at $w(i, j)$, $\sigma_{Rw}^2(i, j)$ is the local variance for Rw and $\sigma_{Rw_{max}}^2$ is the maximum local variances in W .

V. EXPERIMENTAL RESULTS

A. Experimental Setups

During the experiments, the 512×512 test images in Fig. 5 are employed. Fig. 5(m) shows the 512×512 secret pattern to be embedded. For convenience, Steinberg kernel [16] and $\circ = \odot = \text{XNOR}$ will be employed in this paper. Note that in real implementations, CaDEED-N&I will force $y_1(i, j)$ and $y_2(i, j)$ to be identical for $(i, j) \in W_w$ when $X_1 = X_2$.

B. Validation Test

Figs. 6-7 give the validations of CaDEED-EC and CaDEED-N&I. ‘Baboon’ in Fig. 5(a) is employed as the original grayscale image and $X_1 = X_2$. In Fig. 6, Fig. 6(a) and Fig. 6(b) are the generated Y_1 and Y_2 respectively. The AND operation decoded image generated from Y_1 and Y_2 is in Fig. 6(c) and the XNOR operation decoded image is in Fig. 6(d). Similarly, in Fig. 7, Fig. 7(a) and Fig. 7(b) are Y_1 and Y_2 respectively. The AND operation decoded

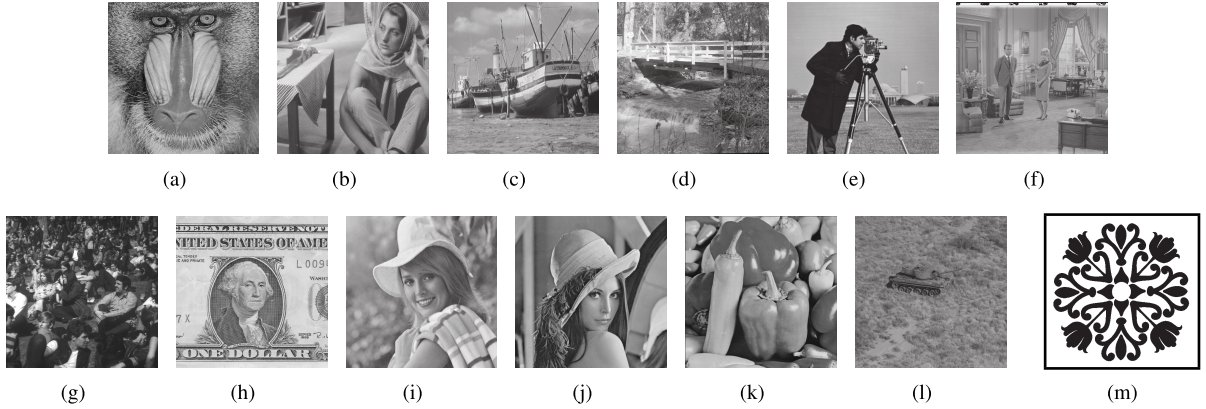


Fig. 5. Test images: (a)'Baboon'; (b)'Barbara'; (c)'Boat'; (d)'Bridge'; (e)'Cameraman'; (f)'Couple'; (g)'Crowd'; (h)'Dollar'; (i)'Elaine'; (j)'Lena'; (k)'Pepper'; (l)'Tank'; (m)Secret pattern to be embedded.

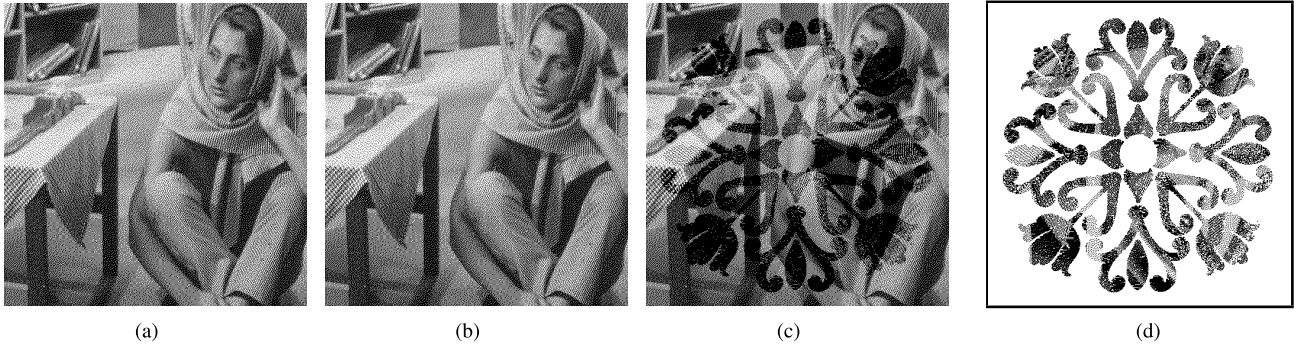


Fig. 6. (a)CaDEED-EC Y_1 . $X_1 = X_2 = \text{'Barbara'}$, Steinberg kernel. (b)CaDEED-EC Y_2 . $X_1 = X_2 = \text{'Barbara'}$, Steinberg kernel. (c)CaDEED-EC AND operation decoded image. $X_1 = X_2 = \text{'Barbara'}$, Steinberg kernel. (d)CaDEED-EC XNOR operation decoded image. $X_1 = X_2 = \text{'Barbara'}$, Steinberg kernel.

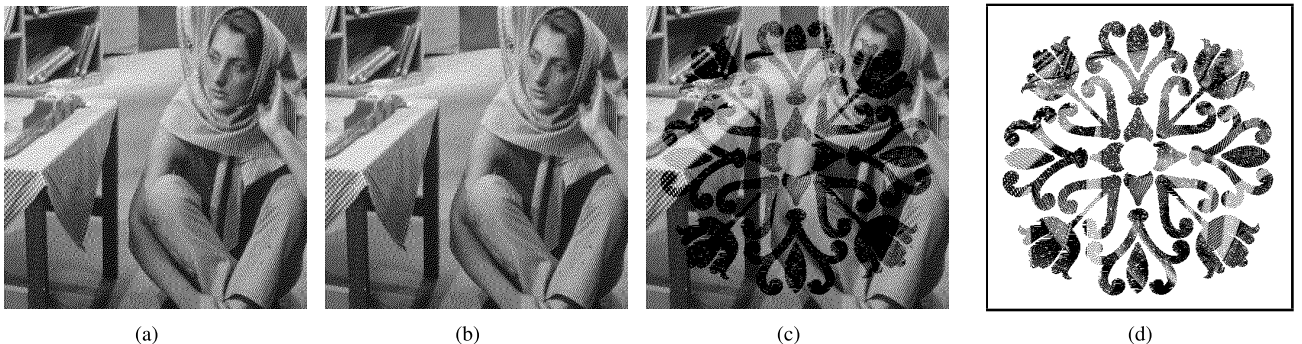


Fig. 7. (a)CaDEED-N&I Y_1 . $X_1 = X_2 = \text{'Barbara'}$, Steinberg kernel. (b)CaDEED-N&I Y_2 . $X_1 = X_2 = \text{'Barbara'}$, Steinberg kernel. (c)CaDEED-N&I AND operation decoded image. $X_1 = X_2 = \text{'Barbara'}$, Steinberg kernel. (d)CaDEED-N&I XNOR operation decoded image. $X_1 = X_2 = \text{'Barbara'}$, Steinberg kernel.

image is in Fig. 7(c). The XNOR operation decoded image is in Fig. 7(d).

As we can observe from Figs. 6-7, both CaDEED-EC and CaDEED-N&I perform well.

C. Parameter Selection

After the validation tests, the local region sizes for the calculation of NVF and IF will be discussed and suggested. The measurement employed in the parameter selection is the Sum of Squared Error (SSE) and the correct decoding rate (CDR).

In CaDEED (DHCED, DHDCED, DEED(L-2) also), the generation process of Y_1 and Y_2 can also be treated equivalently to adding specific noises, which are bounded by

the thresholds, to the original images and carrying out the regular error diffusion process on the noisy images. Therefore, we can calculate SSE as Eq. (43) between the original images and the equivalent noisy images to measure the embedding distortion. Compared to previous modified PSNR, which firstly let the halftone images pass through a low pass filter and then calculate the PSNR between the low-passed halftone images and the original images, this SSE measurement doesn't possess the low-pass filter selection problem and its result will not be affected by the imperfection of the halftoning process, where some embedding distortions may actually improve the measured quality of the stego halftone image.

$$\text{SSE} = \sum(\Delta u_1^2(i, j)) + \sum(\Delta u_2^2(i, j)) \quad (43)$$

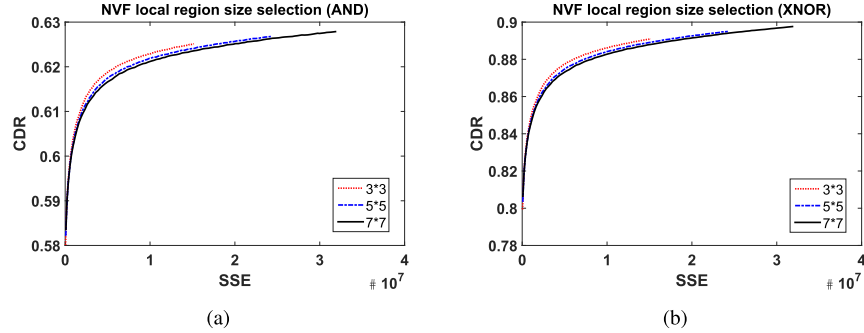


Fig. 8. NVF local region size selection. (a) AND operation decoded results. Steinberg kernel. (b) XNOR operation decoded results. Steinberg kernel.

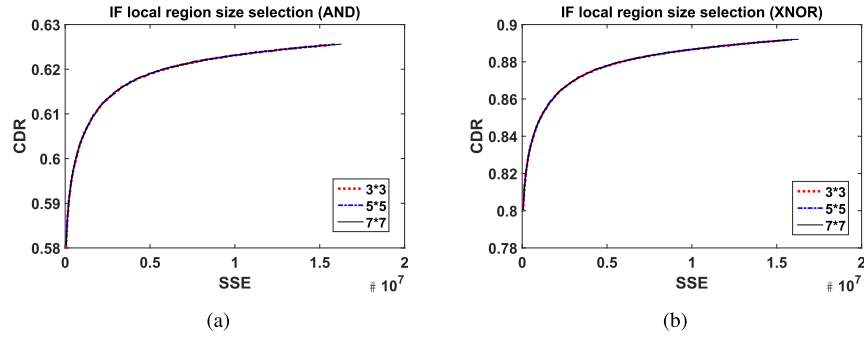


Fig. 9. IF local region size selection. (a) AND operation decoded results. Steinberg kernel. (b) XNOR operation decoded results. Steinberg kernel.

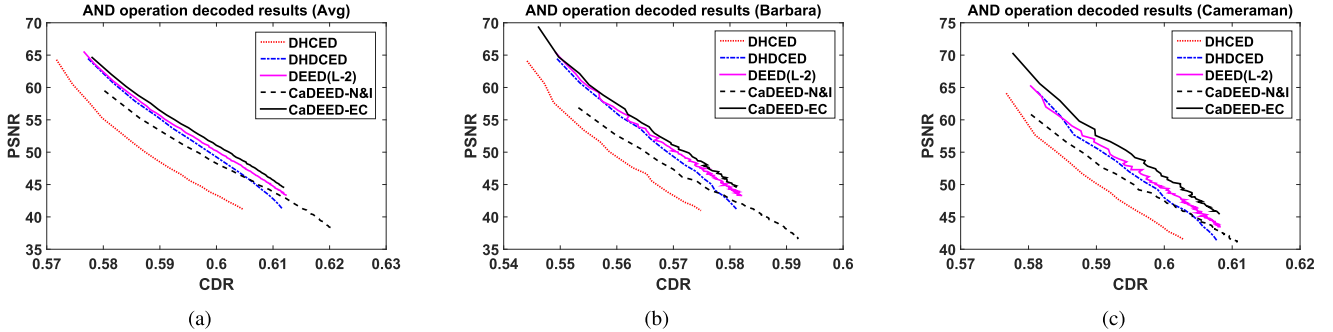


Fig. 10. (a) Average PSNRs of the AND operation decoded results. Steinberg kernel. (b) PSNRs of the AND operation decoded results. $X_1 = X_2 = \text{'Barbara'}$, Steinberg kernel. (c) PSNRs of the AND operation decoded results. $X_1 = X_2 = \text{'Cameraman'}$, Steinberg kernel.

Traditionally, the correct decoding rate (CDR) is utilized to measure the differences between the reference and decoded secret pattern. The CDR is defined as in Eq. (44), where we let D be the decoded image in this paper.

$$\text{CDR} = \frac{\sum |w(i, j) \odot d(i, j)|}{IW \times IH} \quad (44)$$

where IW and IH are the image width and height respectively.

First, the local region size of NVF calculation SR_x is explored. Here, IF is disabled. 3×3 , 5×5 and 7×7 local region sizes are tested and compared. According to the results, $SR_x = 3$ is recommended since it gives the best performance and it possesses the lowest computational complexity. The average results are introduced in Fig. 8.

Then, the local region size of IF SR_w is explored. In this test, the local region size of NVF is set to be 3×3 . Three different sizes 3×3 , 5×5 and 7×7 are tested and compared.

According to the experiments, though the performances of the three tested local region sizes are similar, $SR_w = 3$ is recommended because it possesses the lowest computational complexity. The average results are displayed in Fig. 9.

D. Comparison Test

With CaDEED-N&I's parameters determined, CaDEED-EC and CaDEED-N&I are compared to the classical and latest previous EDHVW methods, DHCED [41], DHDced [45] and DEED(L-2) [39].

Similar to [39], the traditional measurements Peak Signal-to-Noise Ratio (PSNR) and CDR are employed to measure the performances of the EDHVW methods. Figs. 10 and 11 gives the results of DHCED, DHDced, DEED(L-2), CaDEED-EC and CaDEED-N&I. Figs. 10(a) and 11(a) presents the average results, while Figs. 10(b)-10(c) and 11(b)-11(c) introduces the results for specific test images, 'Barbara' and 'Cameraman'.

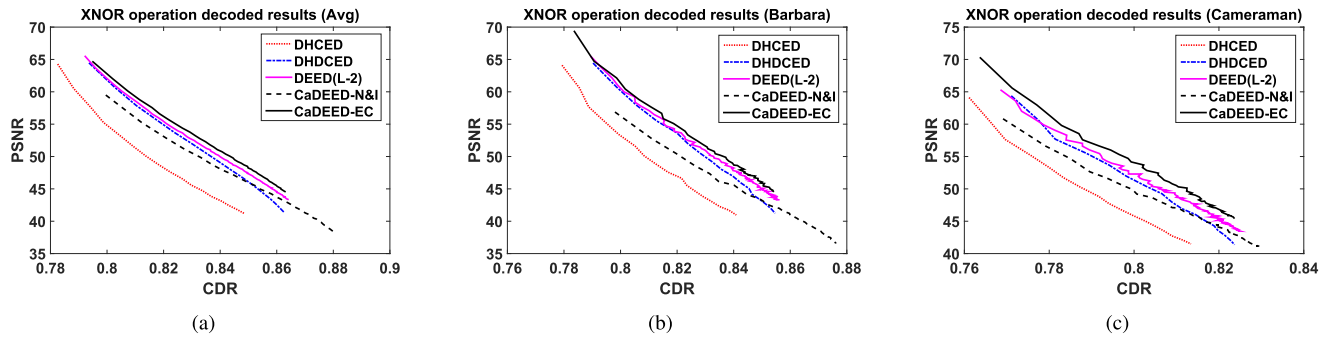


Fig. 11. (a) Average PSNRs of the XNOR operation decoded results. Steinberg kernel. (b) PSNRs of the XNOR operation decoded results. $X_1 = X_2 = \text{‘Barbara’}$, Steinberg kernel. (c) PSNRs of the XNOR operation decoded results. $X_1 = X_2 = \text{‘Camerman’}$, Steinberg kernel.

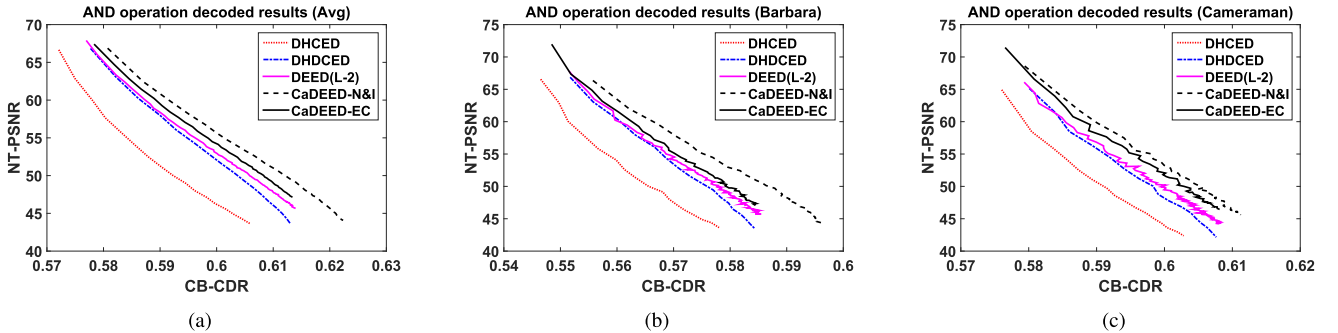


Fig. 12. (a) Average NT-PSNRs of the AND operation decoded results. Steinberg kernel. (b) NT-PSNRs of the AND operation decoded results. $X_1 = X_2 = \text{'Barbara'}$, Steinberg kernel. (c) NT-PSNRs of the AND operation decoded results. $X_1 = X_2 = \text{'Cameraman'}$, Steinberg kernel.

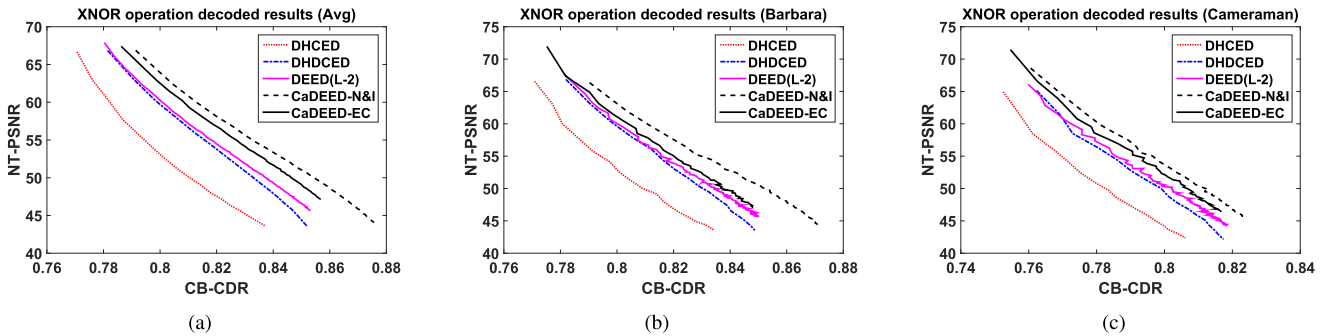


Fig. 13. (a) Average NT-PSNRs of the XNOR operation decoded results. Steinberg kernel. (b) NT-PSNRs of the XNOR operation decoded results. $X_1 = X_2 = \text{'Barbara'}$, Steinberg kernel. (c) NT-PSNRs of the XNOR operation decoded results. $X_1 = X_2 = \text{'Cameraman'}$, Steinberg kernel.

Note that for fair comparison, when we plot these figures, the PSNRs results of DHDCED, DEED(L-2) and CaDEED are the average PSNRs of the two stego images. As we can observe, CaDEED-EC performs obviously better than the previous methods with an approximately 1dB gain when $\text{CB-CDR} = 0.6$ (in Fig. 10(a)), 0.84 (in Fig. 11(a)). Since CaDEED-N&I allows larger distortions for the image regions which contain complex content and PSNR penalizes large distortions more, it is not surprising that its results are not impressive with the traditional measurements.

To better illustrate the superiority of CaDEED-N&I, since complex regions in a image can tolerate more noise than the flat regions, we modify the PSNR measurement in [39] to noise tolerant PSNR (NT-PSNR), which is defined in Eq. (45).

Besides of NT-PSNR, the popular Structural SIMilarity (SSIM) index [48] is also employed to measure the degradations caused by the watermark embedding.

When assessing the extracted secret pattern, the traditional CDR will process every pixel in the secret pattern with equal weights. However, the edge/texture pixels in the secret pattern tend to play a bigger role in maintaining its structure. Therefore, by assigning more weights to those edge/texture pixels, here we propose our new measurement for assessing the decoded secret pattern, which is called the content based correct decoding rate (CB-CDR).

$$\text{CB-CDR} = \frac{\sum (\gamma(i, j) \times |w(i, j) \odot d(i, j)|)}{\sum \gamma(i, j)} \quad (46)$$

Similar to Figs. 10 and 11, Figs. 12(a), 13(a), 14(a) and 15(a) present the average NT-PSNR and SSIM results, while Figs. 12(b)-12(c), 13(b)-13(c), 14(b)-14(c) and 15(b)-15(c) introduces the results for specific test images, ‘Barbara’ and

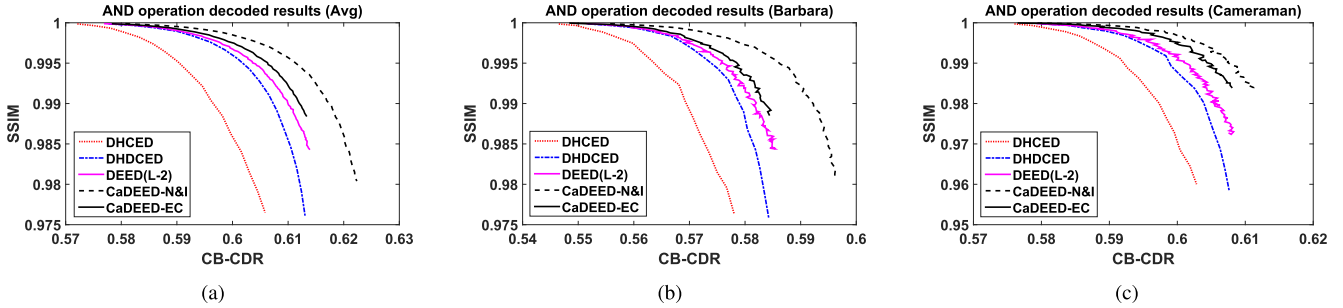


Fig. 14. (a) Average SSIMs of the AND operation decoded results. Steinberg kernel. (b) SSIMs of the AND operation decoded results. $X_1 = X_2 = \text{'Barbara'}$, Steinberg kernel. (c) SSIMs of the AND operation decoded results. $X_1 = X_2 = \text{'Cameraman'}$, Steinberg kernel.

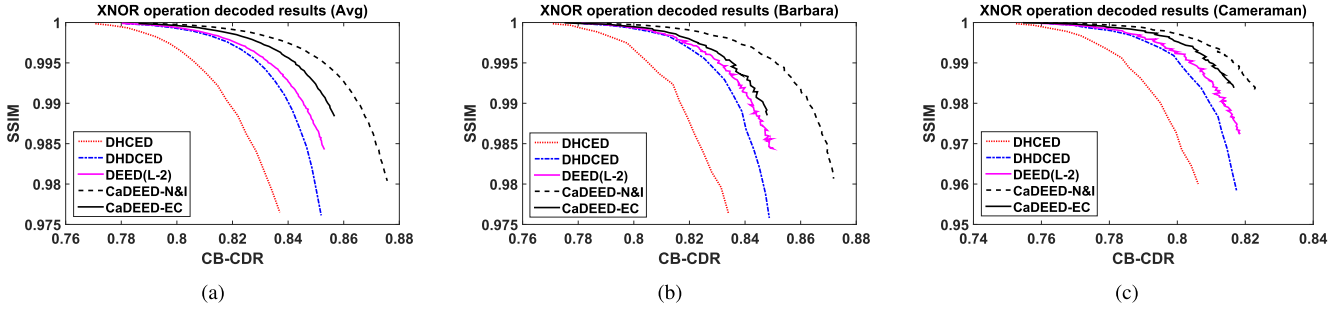


Fig. 15. (a) Average SSIMs of the XNOR operation decoded results. Steinberg kernel. (b) SSIMs of the XNOR operation decoded results. $X_1 = X_2 = \text{'Barbara'}$, Steinberg kernel. (c) SSIMs of the XNOR operation decoded results. $X_1 = X_2 = \text{'Cameraman'}$, Steinberg kernel.

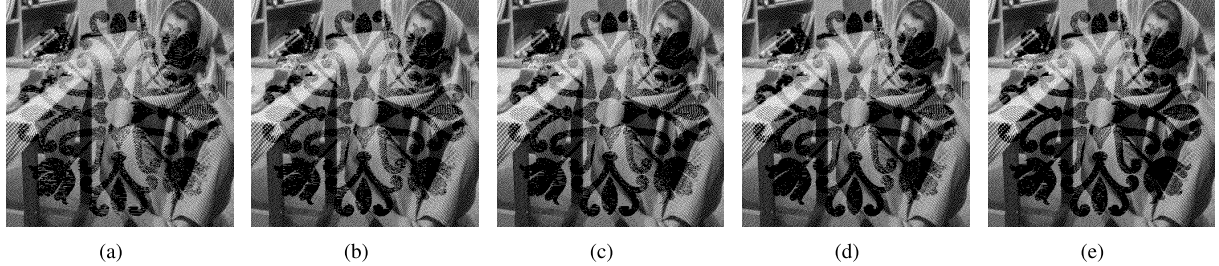


Fig. 16. AND operation decoded images, $X_1 = X_2 = \text{'Barbara'}$, Steinberg kernel. (a) DHCED; (b) DHDced; (c) DEED(L-2); (d) CaDEED-EC; (e) CaDEED-N&I.

'Cameraman'. Note that for fair comparison, when we plot these figures, the NT-PSNRs/SSIMs results of DHDced, DEED(L-2) and CaDEED are the average NT-PSNRs/SSIMs of the two stego images. As we can observe, CaDEED-EC and CaDEED-N&I both perform obviously better than the previous methods. For CB-CDR = 0.6 (in Figs. 12(a) and 14(a)), CaDEED-EC gives an approximately 1.2dB gain in NT-PSNR and 0.08% improvement in SSIM while CaDEED-N&I presents an approximately 2.8dB gain in NT-PSNR and 0.18% improvement in SSIM compared to DEED(L-2). For CB-CDR = 0.84 (in Figs. 13(a) and 15(a)), CaDEED-EC presents an approximately 2.3dB gain in NT-PSNR and 0.29% improvement in SSIM, and CaDEED-N&I gives an approximately 4dB gain in NT-PSNR and 0.47% improvement in SSIM compared to DEED(L-2).

After the numerical comparisons, some visual comparisons will be carried out. Figs. 16-17 presents the revealed secret patterns of DHCED, DHDced, DEED(L-2), CaDEED-EC and CaDEED-N&I, respectively, with the cover images $X_1 = X_2 = \text{'Barbara'}$. With approximately equivalent NT-PSNRs,

Fig. 16 gives the AND operation decoded results, while Fig. 17 reveals the XNOR operation decoded results. As we can observe, CaDEED-EC and CaDEED-N&I give better contrasts of the revealed secret pattern. Note that CaDEED-N&I preserves better fine structures of the watermark. For example, in the lower right region of each decoded image where the lady's left leg co-located, CaDEED-N&I presents the most clear revealed flower pattern among all the results.

E. Discussion of Robustness

In real distribution and transmission process, halftone images mainly suffer from cropping, human-marking attacks and print-and-scan distortions. For cropping or human-marking attacks, part of the decoded secret pattern which has been cropped or human-marked will be lost and others can still be preserved, as the experiment shows in [41].

For the print-and-scan distortions, different watermark decoding approach suffers differently. If the users employ the overlaying (AND) operation for decoding, HVW methods will

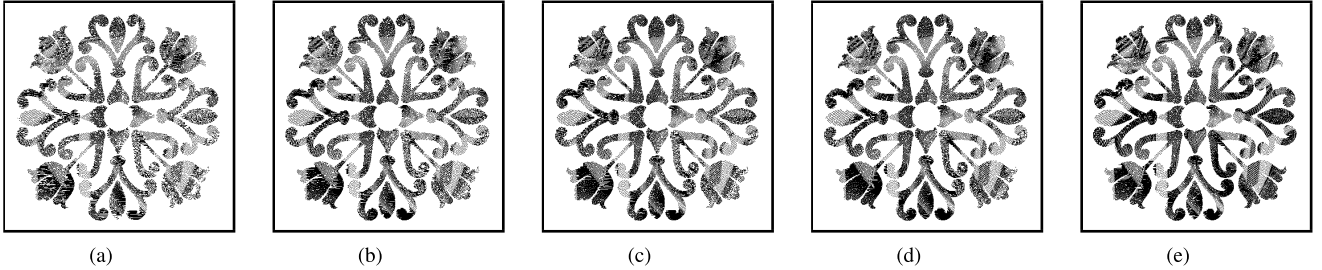


Fig. 17. XNOR operation decoded image, $X_1 = X_2 = \text{'Barbara'}$, Steinberg kernel. (a) DHCED; (b) DHDCE; (c) DEED(L-2); (d) CaDEED-EC; (e) CaDEED-N&I.

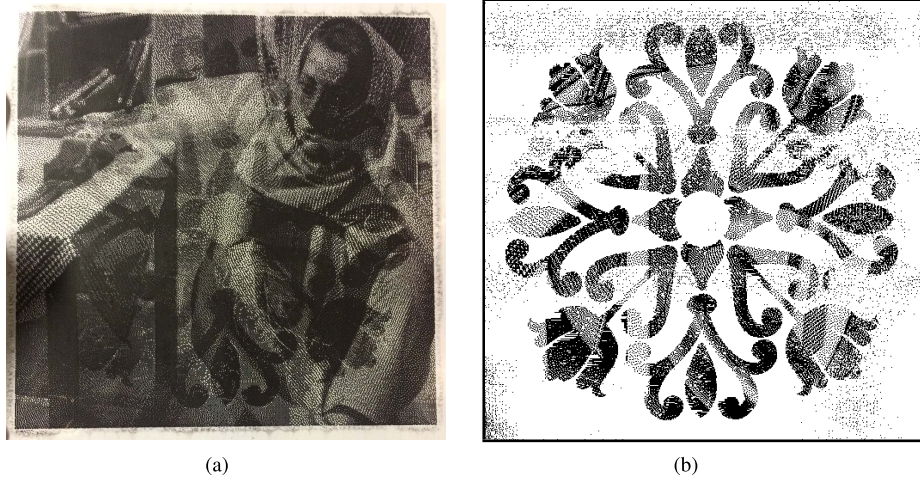


Fig. 18. A real example for CaDEED-N&I. Y_1 and Y_2 are from Figs. 7(a) and 7(b), respectively. (a) AND operation decoded image (which only suffered from print distortions). (b) XNOR operation decoded image (which suffered from print and scan distortions).

usually be affected by the print distortions only, because no scanning is involved during the decoding process. On the other hand, if the users choose to decode the watermark with the XNOR operation, HVW methods will suffer both the print and scan distortions.

Figs. 18 gives a real example, where the stego halftone images Y_1 and Y_2 are from Figs. 7(a) and 7(b), respectively. For Fig. 18(a), Y_1 and Y_2 are printed with a resolution of 96 dot-per-inch (DPI), where the printer model HP LaserJet 4250 is employed, on the transparencies for the convenience of demonstration. Note that we place a white paper below as the background to better show the overlaid result. As we can observe, the overlaid result, i.e. the AND operation decoded result possesses decent decoded watermark result and we can clearly distinguish the majority of the secret pattern. For Fig. 18(b), Y_1 and Y_2 are printed on regular A4 papers with the resolution of 96 DPI and the printer model HP LaserJet 4250. After printing, HP ScanJet G2410 is employed for scanning Y_1 and Y_2 with a resolution of 1200 pixel-per-inch (PPI). Before the XNOR decoding operation is performed, a series of preprocessing steps [39] including rotation, resizing and 1-bit quantization are performed with the help of Adobe Photoshop CS2, to reverse the print-and-scan distortions. As Fig. 18(b) shows, the decoded result reveals most of the secret pattern, though some noise like regions exist. We also measure Fig. 18(b) with CDR and CBCDR. It turns out

that Fig. 18(b) achieves excellent decoding performances with CDR = 82.69% and CBCDR = 82.09%.

VI. CONCLUSION

In this paper, we firstly analyzed the expected performances and limitations of the EDHVW methods. Based on the analysis, we proposed a new general EDHVW method, Content aware Double-sided Embedding Error Diffusion, via considering the expected performances which is affected by the content of the cover images and watermark (secret pattern), the different noise tolerance abilities of different cover image content and the different importance levels of different pixels (when being perceived) in the secret pattern. To demonstrate the effectiveness of the proposed CaDEED, CaDEED-EC and CaDEED-N&I are proposed. CaDEED-EC considered the expected performances only. CaDEED-N&I exploited more by adopting the noise visibility function [47] and proposing the importance factor (IF) for different watermark pixels. In the experiments, the validation tests for CaDEED-EC and CaDEED-N&I were performed first. Then, after selecting the optimal local region sizes for CaDEED-N&I, extensive comparison tests were carried out. The performances were not only measured by the existing PSNR, SSIM and CDR measurements, but also measured by our proposed measurements, NT-PSNR and CB-CDR, to further illustrate the significance of the proposed method. Both the numerical and visual

comparisons indicated that our proposed work outperforms the classical and latest EDHVV methods.

APPENDIX DETAILED DERIVATIONS OF THE ANALYSIS OF EDHVV METHODS

In Section III, the general performance of EDHVV methods is analyzed. Here the omitted detailed derivations of the analysis is presented.

In the left half of R_1 and R_2 , which are in W_w , $y_1(i, j)$ and $y_2(i, j)$ are favored to be identical to each other such that $y_1(i, j)$ and $y_2(i, j)$ tend to be black and white at the same time. To investigate the behavior of $y_A(i, j)$ and $y_O(i, j)$, we consider four different cases separately: (1) $255 \geq A > 127$, $255 \geq B > 127$; (2) $255 \geq A > 127$, $127 \geq B \geq 0$; (3) $127 \geq A \geq 0$, $255 \geq B > 127$; (4) $127 \geq A \geq 0$, $127 \geq B \geq 0$.

From cases (1)-(4) we can conclude that Eq. (47)-(50) can effectively describe the probability distribution for cases (1)-(4), while Eq. (51) and (52) describe the expectations of Y_A and Y_O where $(i, j) \in W_w$.

$$\begin{aligned} P[y_A(i, j) = 255] &= P[y_1(i, j) = 255 \cap y_2(i, j) = 255] \\ &\approx \min(P[y_1(i, j) = 255], \\ &\quad P[y_2(i, j) = 255]) \\ &= \frac{\min(A, B)}{255} \end{aligned} \quad (47)$$

$$P[y_A(i, j) = 0] \approx \frac{255 - \min(A, B)}{255} \quad (48)$$

$$\begin{aligned} P[y_O(i, j) = 255] &= P[(y_1(i, j) \odot y_2(i, j)) = 255] \\ &\approx \frac{255 - |A - B|}{255} \end{aligned} \quad (49)$$

$$P[y_O(i, j) = 0] \approx \frac{|A - B|}{255} \quad (50)$$

Then

$$\begin{aligned} E[y_A(i, j)] &= 0 \cdot P[y_A(i, j) = 0] + 255 \cdot P[y_A(i, j) = 255] \\ &\approx 0 \cdot \frac{\min(A, B)}{255} + 255 \cdot \frac{255 - \min(A, B)}{255} \\ &= 255 - \min(A, B), \end{aligned} \quad (51)$$

$$\begin{aligned} E[y_O(i, j)] &= 0 \cdot P[y_O(i, j) = 0] + 255 \cdot P[y_O(i, j) = 255] \\ &\approx 0 \cdot \frac{|A - B|}{255} + 255 \cdot \frac{255 - |A - B|}{255} \\ &= 255 - |A - B|. \end{aligned} \quad (52)$$

In the right half of R_1 and R_2 , which are in W_b , $y_1(i, j)$ and $y_2(i, j)$ are favored to be conjugate to each other such that $y_1(i, j)$ and $y_2(i, j)$ tend not to be black at the same time. To investigate the behavior of $y_A(i, j)$ and $y_O(i, j)$, we also consider four different cases: (1) $255 \geq A > 127$, $255 \geq B > 127$; (2) ($255 \geq A > 127$, $127 \geq B \geq 0$ or $127 \geq A \geq 0$, $255 \geq B > 127$) and $A + B \leq 255$; (3) ($255 \geq A > 127$, $127 \geq B \geq 0$ or $127 \geq A \geq 0$, $255 \geq B > 127$) and $A + B > 255$; (4) $127 \geq A \geq 0$, $127 \geq B \geq 0$. After we divide the problem into cases (1)-(4), we can combine the four cases as two cases: (1) $A + B > 255$, (2) $A + B \leq 255$.

For case(1), there are more white pixels than black pixels in both R_1 and R_2 . The percentage of black pixels in the

right half of R_1 of Y_1 is about $(255 - A)/255 \cdot 100\%$. The percentage of black pixels in the right half of R_2 of Y_2 is about $(255 - B)/255 \cdot 100\%$. Consider the situation that the black pixels in the right half of R_1 and the black pixels in the right half of R_2 are at different locations since $y_1(i, j)$ and $y_2(i, j)$ tend not to be black at the same time when $(i, j) \in W_b$. Then

$$\begin{aligned} P[y_A(i, j) = 0] &= P[y_1(i, j) = 0] + P[y_2(i, j) = 0] \\ &\approx \frac{255 - A}{255} + \frac{255 - B}{255} \\ &= \frac{2 \cdot 255 - A - B}{255}, \end{aligned} \quad (53)$$

$$P[y_A(i, j) = 255] \approx \frac{A + B - 255}{255}, \quad (54)$$

$$P[y_O(i, j) = 0] = P[y_A(i, j) = 0] \approx \frac{2 \cdot 255 - A - B}{255}, \quad (55)$$

$$P[y_O(i, j) = 255] = P[y_A(i, j) = 255] \approx \frac{A + B - 255}{255}. \quad (56)$$

Then

$$\begin{aligned} E[y_A(i, j)] &= 0 \cdot P[y_A(i, j) = 0] + 255 \cdot P[y_A(i, j) = 255] \\ &\approx 0 \cdot \frac{2 \cdot 255 - A - B}{255} + 255 \cdot \frac{A + B - 255}{255} \\ &= A + B - 255, \end{aligned} \quad (57)$$

$$\begin{aligned} E[y_O(i, j)] &= 0 \cdot P[y_O(i, j) = 0] + 255 \cdot P[y_O(i, j) = 255] \\ &\approx 0 \cdot \frac{2 \cdot 255 - A - B}{255} + 255 \cdot \frac{A + B - 255}{255} \\ &= A + B - 255. \end{aligned} \quad (58)$$

Consequently, the contrasts C_s between the left and right halves of R in Y_A and Y_O can be expressed as

$$\begin{aligned} C_{sA} &= \frac{E[y_A(i, j)|(i, j) \in W_w] - E[y_A(i, j)|(i, j) \in W_b]}{E[y_A(i, j)|(i, j) \in W_w]} \\ &= \frac{255 - \min(A, B) - (A + B - 255)}{255 - \min(A, B)}, \end{aligned} \quad (59)$$

$$\begin{aligned} C_{sO} &= \frac{E[y_O(i, j)|(i, j) \in W_w] - E[y_O(i, j)|(i, j) \in W_b]}{E[y_O(i, j)|(i, j) \in W_w]} \\ &= \frac{255 - |A - B| - (A + B - 255)}{255 - |A - B|}. \end{aligned} \quad (60)$$

For case(2), there are more black pixels than white pixels in R_1 and R_2 . Consider the situation that the black pixels in the right half of R_1 and the black pixels in the right half of R_2 are at different locations, except $\frac{255-A}{255} \cdot 100\% + \frac{255-B}{255} \cdot 100\% - 1 \cdot 100\%$ percent of pixel pairs which can only both be black. Then

$$P[y_A(i, j) = 0] = P[y_1(i, j) = 0 \cup y_2(i, j) = 0] \approx 1, \quad (61)$$

$$P[y_A(i, j) = 255] = P[y_1(i, j) = 255 \cap y_2(i, j) = 255] \approx 0 \quad (62)$$

$$\begin{aligned} P[y_O(i, j) = 0] &= P[(y_1(i, j) \odot y_2(i, j)) = 0] \\ &\approx 1 \cdot 100\% - \left(\frac{255 - A}{255} \cdot 100\%\right. \\ &\quad \left.+ \frac{255 - B}{255} \cdot 100\% - 1 \cdot 100\%\right) \\ &= \frac{A + B}{255}, \end{aligned} \quad (63)$$

$$P[y_O(i, j) = 255] \approx \frac{255 - (A + B)}{255}. \quad (64)$$

Then

$$\begin{aligned} E[y_A(i, j)] &= 0 \cdot P[y_A(i, j) = 0] + 255 \cdot P[y_A(i, j) = 255] \\ &\approx 0 \cdot 1 + 255 \cdot 0 \\ &= 0, \end{aligned} \quad (65)$$

$$\begin{aligned} E[y_O(i, j)] &= 0 \cdot P[y_O(i, j) = 0] + 255 \cdot P[y_O(i, j) = 255] \\ &\approx 0 \cdot \frac{A + B}{255} + 255 \cdot \frac{255 - (A + B)}{255} \\ &= 255 - (A + B). \end{aligned} \quad (66)$$

Consequently, the contrasts C_s between the left and right halves of R in Y_A and Y_O can be expressed as

$$\begin{aligned} C_{sA} &= \frac{E[y_A(i, j)|(i, j) \in W_w] - E[y_A(i, j)|(i, j) \in W_b]}{E[y_A(i, j)|(i, j) \in W_w]} \\ &= \frac{255 - \min(A, B) - 0}{255 - \min(A, B)} \\ &= 1, \end{aligned} \quad (67)$$

$$\begin{aligned} C_{sO} &= \frac{E[y_O(i, j)|(i, j) \in W_w] - E[y_O(i, j)|(i, j) \in W_b]}{E[y_O(i, j)|(i, j) \in W_w]} \\ &= \frac{255 - |A - B| - (255 - (A + B))}{255 - |A - B|}. \end{aligned} \quad (68)$$

Then Eqs. (17)-(22) can be summarized.

REFERENCES

- [1] M. U. Celik, G. Sharma, E. Saber, and A. M. Tekalp, "Hierarchical watermarking for secure image authentication with localization," *IEEE Trans. Image Process.*, vol. 11, no. 6, pp. 585–595, Jun. 2002.
- [2] E. Walia, A. Suneja, "Fragile and blind watermarking technique based on Weber's law for medical image authentication," *IET Comput. Vis.*, vol. 7, no. 1, pp. 9–19, Feb. 2013.
- [3] C.-J. Cheng, W.-J. Hwang, H.-Y. Zeng, and Y.-C. Lin, "A fragile watermarking algorithm for hologram authentication," *J. Display Technol.*, vol. 10, no. 4, pp. 263–271, Apr. 2014.
- [4] X. Cao, L. Du, X. Wei, D. Meng, and X. Guo, "High capacity reversible data hiding in encrypted images by patch-level sparse representation," *IEEE Trans. Cybern.*, vol. 46, no. 5, pp. 1132–1143, May 2016.
- [5] E. Nezhadarya, Z. J. Wang, and R. K. Ward, "Robust image watermarking based on multiscale gradient direction quantization," *IEEE Trans. Inf. Forensics Security*, vol. 6, no. 4, pp. 1200–1213, Dec. 2011.
- [6] A. V. Subramanyam, S. Emmanuel, and M. S. Kankanhalli, "Robust watermarking of compressed and encrypted JPEG2000 images," *IEEE Trans. Multimedia*, vol. 14, no. 3, pp. 703–716, Jun. 2012.
- [7] H.-D. Kim, J.-W. Lee, T.-W. Oh, and H.-K. Lee, "Robust DT-CWT watermarking for DIBR 3D images," *IEEE Trans. Broadcast.*, vol. 58, no. 4, pp. 533–543, Dec. 2012.
- [8] J. Wang, S. Lian, and Y.-Q. Shi, "Hybrid multiplicative multi-watermarking in DWT domain," *Multidimensional Syst. Signal Process.*, vol. 28, no. 2, pp. 617–636, Apr. 2017.
- [9] T. Zong, Y. Xiang, I. Natgunanathan, S. Guo, W. Zhou, and G. Beliakov, "Robust histogram shape-based method for image watermarking," *IEEE Trans. Circuits Syst. Video Technol.*, vol. 25, no. 5, pp. 717–729, May 2015.
- [10] C. Yuan, Z. Xia, and X. Sun, "Coverless image steganography based on SIFT and BOF," *J. Internet Technol.*, vol. 18, no. 2, pp. 435–442, Mar. 2017.
- [11] X. Chen, S. Chen, and Y. Wu, "Coverless information hiding method based on the Chinese character encoding," *J. Internet Technol.*, vol. 18, no. 2, pp. 313–320, Mar. 2017.
- [12] L. Xiong, Z. Xu, and Y.-Q. Shi, "An integer wavelet transform based scheme for reversible data hiding in encrypted images," *Multidimensional Syst. Signal Process.*, vol. 29, no. 3, pp. 1191–1202, 2018.
- [13] Y.-Y. Chen, T. Kashti, M. Fischer, D. Shaked, R. Ulichney, and J. P. Allebach, "The lattice-based screen set: A square N-color all-orders moiré-free screen set," *IEEE Trans. Image Process.*, vol. 25, no. 4, pp. 1873–1886, Apr. 2016.
- [14] X. Zhang, A. Veis, R. Ulichney, and J. P. Allebach, "Multilevel halftone screen design: Keeping texture or keeping smoothness?" in *Proc. IEEE Int. Conf. Image Process.*, Sep. 2012, pp. 829–832.
- [15] B. E. Bayer, "An optimum method for two level rendition of continuous tone pictures," in *Proc. IEEE Int. Commun. Conf.*, Jun. 1973, pp. 2611–2615.
- [16] R. W. Floyd and L. Steinberg, "An adaptive algorithm for spatial grayscale," in *Proc. Soc. Inf. Display*, 1976, pp. 75–77.
- [17] J. F. Jarvis, C. N. Judice, and W. Ninke, "A survey of techniques for the display of continuous tone pictures on bilevel displays," *Comput. Graph. Image Process.*, vol. 5, no. 1, pp. 13–40, 1976.
- [18] X. Li, "Edge-directed error diffusion halftoning," *IEEE Signal Process. Lett.*, vol. 13, no. 11, pp. 688–690, Nov. 2006.
- [19] D. E. Knuth, "Digital halftones by dot diffusion," *ACM Trans. Graph.*, vol. 6, no. 4, pp. 245–273, Oct. 1987.
- [20] M. Mese and P. P. Vaidyanathan, "Optimized halftoning using dot diffusion and methods for inverse halftoning," *IEEE Trans. Image Process.*, vol. 9, no. 4, pp. 691–709, Apr. 2000.
- [21] J.-M. Guo and Y.-F. Liu, "Improved dot diffusion by diffused matrix and class matrix co-optimization," *IEEE Trans. Image Process.*, vol. 18, no. 8, pp. 1804–1816, Aug. 2009.
- [22] Y.-F. Liu and J.-M. Guo, "New class tiling design for dot-diffused halftoning," *IEEE Trans. Image Process.*, vol. 22, no. 3, pp. 1199–1208, Mar. 2013.
- [23] S. H. Kim and J. P. Allebach, "Impact of HVS models on model-based halftoning," *IEEE Trans. Image Process.*, vol. 11, no. 3, pp. 258–269, Mar. 2002.
- [24] P. Goyal, M. Gupta, C. Staelin, M. Fischer, O. Shacham, and J. P. Allebach, "Clustered-dot halftoning with direct binary search," *IEEE Trans. Image Process.*, vol. 22, no. 2, pp. 473–487, Feb. 2013.
- [25] J.-M. Guo, Y.-F. Liu, and J.-Y. Chang, "High efficient direct binary search using multiple lookup tables," in *Proc. Int. Conf. Image Process.*, Sep. 2013, pp. 813–816.
- [26] X. Zhang and J. P. Allebach, "Quad-interleaved block level parallel direct binary search algorithm," *Electron. Imag.*, vol. 20, pp. 1–6, Feb. 2016.
- [27] P. Moulin and R. Koetter, "Data-hiding codes," *Proc. IEEE*, vol. 93, no. 12, pp. 2083–2126, Dec. 2005.
- [28] M. S. Fu and O. C. Au, "Data hiding by smart pair toggling for halftone images," in *Proc. IEEE Int. Conf. Acoust., Speech, Signal Process.*, Jun. 2000, pp. 2318–2321.
- [29] M. S. Fu and O. C. Au, "Halftone image data hiding with intensity selection and connection selection," *Signal Process.: Image Commun.*, vol. 16, no. 10, pp. 909–930, Aug. 2001.
- [30] M. S. Fu and O. C. Au, "Data hiding watermarking for halftone images," *IEEE Trans. Image Process.*, vol. 11, no. 4, pp. 477–484, Apr. 2002.
- [31] S.-C. Pei and J.-M. Guo, "High-capacity data hiding in halftone images using minimal-error bit searching and least-mean square filter," *IEEE Trans. Image Process.*, vol. 15, no. 6, pp. 1665–1679, Jun. 2006.
- [32] O. Bulan, G. Sharma, and V. Monga, "Orientation modulation for data hiding in clustered-dot halftone prints," *IEEE Trans. Image Process.*, vol. 19, no. 8, pp. 2070–2084, Aug. 2010.
- [33] J.-M. Guo and Y.-F. Liu, "Halftone-image security improving using overall minimal-error searching," *IEEE Trans. Image Process.*, vol. 20, no. 10, pp. 2800–2812, Oct. 2011.
- [34] Y. Guo, O. C. Au, K. Tang, L. Fang, and Z. Yu, "Data hiding in dot diffused halftone images," in *Proc. IEEE Int. Conf. Multimedia Expo*, Jul. 2011, pp. 1–6.
- [35] Y. Guo *et al.*, "Data hiding in error diffused color halftone images," in *Proc. IEEE Int. Symp. Circuits Syst.*, May 2013, pp. 2996–2999.
- [36] Y. Guo, O. C. Au, K. Tang, and J. Pang, "Hiding a secret pattern into color halftone images," in *Digital-Forensics and Watermarking*. Berlin, Germany: Springer, 2014, pp. 465–474.
- [37] S. Sachdev, A. Nayak, and T. Pradhan, "Data hiding in halftone images using mathematical morphology and conjugate ordered dithering," in *Proc. Int. Conf. High Perform. Comput. Appl.*, Dec. 2014, pp. 1–7.
- [38] Y. Guo, O. C. Au, and K. Tang, "Watermark embedding for multi-scale error diffused halftone images by adopting visual cryptography," *Int. J. Digit. Crime Forensics*, vol. 7, no. 1, pp. 51–68, Jan. 2015.
- [39] Y. Guo, O. C. Au, J. Zhou, K. Tang, and X. Fan, "Halftone image watermarking via optimization," *Signal Process.: Image Commun.*, vol. 41, pp. 85–100, Feb. 2016.
- [40] M. S. Fu and O. C. Au, "Data hiding in halftone images by stochastic error diffusion," in *Proc. IEEE Int. Conf. Acoust., Speech, Signal Process.*, May 2001, pp. 1965–1968.

- [41] M. S. Fu and O. C. Au, "Steganography in halftone images: Conjugate error diffusion," *Signal Process.*, vol. 83, no. 10, pp. 2171–2178, Oct. 2003.
- [42] S.-C. Pei and J.-M. Guo, "Data hiding in halftone images with noise-balanced error diffusion," *IEEE Signal Process. Lett.*, vol. 10, no. 12, pp. 349–351, Dec. 2003.
- [43] C. C. Chang, C. S. Chan, and W. L. Tai, "Hiding a halftone secret image in two camouflaged halftone images," *Pattern Recognit. Image Anal.*, vol. 16, no. 3, pp. 486–496, Jul. 2006.
- [44] C.-N. Yang, Y.-Y. Yang, T.-S. Chen, and G.-C. Ye, "New steganography scheme in halftone images," in *Proc. IEEE Int. Conf. Intell. Inf. Hiding Multimedia Signal Process.*, Aug. 2008, pp. 1520–1523.
- [45] Y. Guo, O. C. Au, L. Fang, and K. Tang, "Data hiding in halftone images by dual conjugate error diffusion," in *Proc. Asia-Pacific Signal Inf. Process. Assoc. Annu. Summit Conf.*, 2011, pp. 1–4.
- [46] J.-M. Guo and J.-J. Tsai, "Data-hiding in halftone images using adaptive noise-balanced error diffusion," *IEEE Multimedia*, vol. 18, no. 2, pp. 48–59, Feb. 2011.
- [47] S. Voloshynovskiy, A. Herrigel, N. Baumgaertner, and T. Pun, "A stochastic approach to content adaptive digital image watermarking," in *Information Hiding*. Berlin, Germany: Springer, 2000.
- [48] Z. Wang, A. C. Bovik, H. R. Sheikh, and E. P. Simoncelli, "Image quality assessment: From error visibility to structural similarity," *IEEE Trans. Image Process.*, vol. 13, no. 4, pp. 600–612, Apr. 2004.



Rui Wang received the B.S. degree from Tsinghua University, Beijing, China, in 2005, and the Ph.D. degree from the University of Chinese Academy of Sciences, Beijing, China, in 2011. She is currently a Professor with the State Key Laboratory of Information Security, Institute of Information Engineering, Chinese Academy of Sciences, Beijing, China. Her research interests include image/video processing, image retrieval, and object detection.



Yuanfang Guo received the B.S. and Ph.D. degrees from The Hong Kong University of Science and Technology, Hong Kong, in 2009 and 2015, respectively. He is currently an Assistant Professor with the State Key Laboratory of Information Security, Institute of Information Engineering, Chinese Academy of Sciences, Beijing, China. His research interests include image/video watermarking, data hiding, forensics, compression, restoration, and enhancement.



Lu Fang received the Ph.D. degree in electronic and computer engineering from The Hong Kong University of Science and Technology in 2011, and the B.E. degree from USTC in 2007. He is currently an Associate Professor with the Tsinghua-Berkeley Shenzhen Institute, Tsinghua University. His current research interests include computational photography and visual computing.



Oscar C. Au (F'12) received the B.A.Sc. degree from the University of Toronto in 1986 and the M.A. and Ph.D. degrees from Princeton University in 1988 and 1991, respectively. He held a postdoctoral position at Princeton University for one year. In 1992, he joined The Hong Kong University of Science and Technology (HKUST) as an Assistant Professor and promoted to an Associate Professor and then a Full Professor. In 2014, he left HKUST and migrated to USA. He is currently the Vice President of Origin Wireless Inc.

His main research contributions are on video/image coding and processing, watermarking/light weight encryption, and speech/audio processing. He has authored 70 technical journal papers, over 370 conference papers, three book chapters, and over 70 contributions to international standards.

Dr. Au is a fellow of the HKIE. He is/was an Associate/Senior Editor of several IEEE journals, such as TCSVT, TIP, TCAS1, SPL, JSTSP, and SigView, and non-IEEE journals such as, JVCIR, JSPS, TSIP, JMM, JFI, and SWJ. He is a guest editor of some special issues in JSTSP and TCSVT. He was a BoG Member and the Vice President C Technical Activity of APSIPA. He was the Chair of three technical committees, such as IEEE CAS MSA TC, IEEE SPS MMSP TC, and APSIPA IVM TC. He was a member of five other TCs, such as the IEEE CAS VSPC TC, DSP TC, IEEE SPS IVMS TC, IFS TC, and IEEE ComSoc MMC TC. He served on two steering committees, such as the IEEE TMM and IEEE ICME. He also served on organizing committee of many conferences, including ISCAS 1997, ICASSP 2003, ISO/IEC 71st MPEG in 2005, and ICIP 2010. He was the General Chair of several conferences, such as PCM 2007, ICME 2010, and PV 2010. He was a recipient of five best paper awards, such as SiPS 2007, PCM 2007, MMSP 2012, ICIP 2013, and MMSP 2013. He was an IEEE Distinguished Lecturer (DL) in 2009 and 2010, respectively, and APSIPA DL in 2013 and 2014, respectively. He has been a keynote speaker multiple times.



Xiaochun Cao received the B.S. and M.S. degrees in computer science from Beihang University, Beijing, China, and the Ph.D. degree in computer science from the University of Central Florida, Orlando, FL, USA. He spent about three years at ObjectVideo Inc., as a Research Scientist. From 2008 to 2012, he was a Professor with Tianjin University, Tianjin, China. He is currently a Professor with the Institute of Information Engineering, Chinese Academy of Sciences, Beijing, China. He has authored and co-authored over 170 journal and conference papers.

Dr. Cao is a fellow of the IET. He is on the Editorial Board of the IEEE TRANSACTIONS ON IMAGE PROCESSING and the IEEE TRANSACTIONS ON CIRCUITS AND SYSTEMS FOR VIDEO TECHNOLOGY. His dissertation was nominated for the University of Central Florida's University-Level Outstanding Dissertation Award. He was a recipient of the Piero Zamperoni Best Student Paper Award at the International Conference on Pattern Recognition in 2004 and 2010, respectively.